Federated Cell-Free MIMO in Nonterrestrial Networks: Architectures and Performance

ALESSANDRO GUIDOTTI , Member, IEEE
Consorzio Nazionale Interuniversitario per le Telecomunicazioni, Parma, Italy

ALESSANDRO VANELLI-CORALLI , Senior Member, IEEE
CARLA AMATETTI , Member, IEEE
University of Bologna, Bologna, Italy

While 5G networks are being rolled out, the definition of 5G-advanced features and the identification of disruptive technologies for 6G systems are being addressed by the scientific and academic communities to tackle the challenges that 2030 communication systems will face, such as terabit capacity and always-ON networks. In this framework, it is globally recognized that nonterrestrial networks (NTN) will play a fundamental role in support to a fully connected world, in which physical, human, and digital domains will converge. Notably, one of the main challenges that NTN have to address is the provision of the high throughput requested by the new ecosystem. In this article, we focus on cell-free massive multiple input multiple output (CF-MIMO) algorithms for NTN. In particular: we discuss the architecture design supporting centralized and federated CF-MIMO in NTN, with the latter implementing distributed MIMO algorithms from multiple satellites in the same formation (swarm), we design a location-based CF-MIMO algorithm, which does not require channel state information at the transmitter, and we design normalization approaches for federated CF-MIMO in NTN, to cope with the constraints on noncolocated radiating elements. The numerical results substantiate the good performance of the proposed algorithm, also in the presence of nonideal information.

I. INTRODUCTION

During the last years, telecommunication networks experienced an unprecedented request for an ever increasing throughput, combined with the need to support very diverse services with heterogeneous performance requirements in terms of data rate and latency. While ultrareliable and low latency communications, massive machine-type communications, and enhanced mobile broadband 5G services are being provided with global benefit for both economy and society, the design of new features for 5G-advanced (5G-A) and the research on 6G technologies are already ongoing [1], [2], [3], [4]. Since 2021, ITU-R initiated the development of the vision for IMT-2030 and beyond within working party 5D [5]; these activities are being performed in synergy with the ITU-T Focus Group Technologies for Network 2030, which, between 2018 and 2020, identified a preliminary set of target services for 6G communications [6]. The envisioned 6G system will support a fully connected world, characterized by the convergence of the physical, human, and digital domains [7], [8]. According to the 6G Infrastructure Association, three broad classes of services can be foreseen [9], as follows.

1) Digital twinning, of the systems, with actuators and sensors tightly synchronizing the abovementioned domains to create digital twins of cities, factories, or even bodies.
2) Connected intelligence, in which the network serves as the cornerstone through which trusted artificial intelligence (AI) functions can manage the virtual representations in the digital domain.
3) Immersive communications, in which high/ultrahigh resolution visual/spatial, tactile/haptic, and other sensory data can be exchanged to create a fully immersive experience.

In the above context, service ubiquity and continuity are critical features that only the full and seamless integration of terrestrial and nonterrestrial networks (NTN) can enable [10], [11], [12], [13], [14], [15]. The NTN segment will complete the overall system architecture by providing a ubiquitous, continuous, flexible, and resilient infrastructure for the following:

1) direct connectivity to smartphones in outdoor and in-vehicle (emergency communications) scenarios;
2) connectivity to mobile platforms (trains, planes, ships, drones);
3) broadcast/multicast services;
4) low latency communications to support vertical markets (e.g., railway, automotive, and aeronautical);
5) Internet of Things applications;
6) support to precise network-based positioning.

A key enabler of the NTN communication infrastructure will be the support for high throughput communications. Current geostationary Earth orbit (GEO) high throughput satellite (HTS) systems provide hundred of Gbps through

multibeam (MB) coverage [16], [17]. Typically, these systems are based on multicolor, e.g., three or four colors, frequency reuse schemes in which the available bandwidth is split into multiple nonoverlapping spectrum chunks and assigned on a geographic basis to limit interference. However, further improvements are needed to achieve the envisioned very HTS with terabit capacity. Several commercial endeavors are targeting the deployment of GEO systems with thousands of spot beams [18]. Moreover, also low EO (LEO) megaconstellations, which ease the closure of the link budget and reduce the propagation delay, have been receiving increasing interest and some of them have started the services [19], [20], [21]. Since current physical layer technologies already achieved a spectral efficiency close to the theoretical Shannon limit, the emphasis for future NTN systems is being placed on system design approaches aiming at increasing the exploitation of the available spectrum by means of advanced spectrum usage paradigms, e.g., dynamic spectrum access [11], or cognitive radios [22], [23], or by decreasing the frequency reuse factor down full frequency reuse (FFR). Notably, the latter shall be combined with effective interference management techniques, such as beamforming, precoding, and multiple input multiple output (MIMO) to exploit the massive generated co-channel interference.

In the past years, the exploitation of antenna arrays through beamforming, precoding, and MIMO techniques in NTN has been extensively addressed, as discussed in the next section. These works, as detailed in the next section, focused on the increase of the system throughput in different scenarios, including unicast or multicast transmissions, ideal and nonideal channel state information (CSI) at the transmitter, geosynchronous and, more recently, nonGeoSynchronous Orbit (NGSO) systems, and advanced radio resource management (RRM) algorithms. In this article, we advance from that by addressing the design and performance of cell-free (CF) MIMO in NGSO-based NTN, considering both centralized architectures, i.e., MIMO with colocated radiating elements on-board a single satellite, and federated solutions, i.e., MIMO with non colocated radiating elements on-board multiple satellites belonging to the same formation. It is worthwhile highlighting that, in the framework of NTN systems, the term CF refers to not requiring the definition of a beam lattice on-ground, thus computing the beamforming coefficients based on the channel between the on-board radiating elements (rather than the equivalent beam antennas) and the users.

A. Literature Review

The literature on the application of MIMO supported by precoding and digital beamforming to NTN systems is extensive; in fact, based on the impressive benefit brought by MIMO solutions to terrestrial communications, their application to satellite communications has been one of the most discussed research areas in the past years. Initially, the considered multi-user MIMO techniques were based on the implementation of zero forcing and minimum mean square error (MMSE) MIMO in satellite scenarios [24]; this work showed that throughput gains in the order of 80% could be obtained on both the forward and the return links. Arapoglou et al. [25] provided a detailed and complete survey on the application of MIMO techniques over satellite channels; both fixed and mobile satellite communications were addressed, also identifying the most impacting channel impairments. Zorba et al. [26] discussed the availability of only partial, and not full, CSI at the transmitter side, which is one of the most critical challenges in satellite-based MIMO. In addition to this valuable insight, the authors also introduce a novel MIMO scheme aimed at increasing the sum rate and availability. Building on this momentum, also several projects funded by the European Space Agency addressed the implementation of precoding to the DVB-S2X standard [27]; more specifically, the following practical challenges arising for MIMO in HTS systems were discussed: framing issues, nonideal phase estimates, nonideal CSI at the transmitter due to imperfect estimation at the user terminal, and the impact of multiple gateways (GWs). The practical impairments in the application of MIMO to DVB-S2X-based systems were also discussed in [28] and the studies in [29] and [30] provide a thorough review of precoding solutions for MB satellite systems; in these latter works, the optimization of the precoder design with linear and nonlinear power constraint is also discussed. In [31], the nonlinear Tomlinson–Harashima precoding is proposed. The performance of linear precoding, when also taking into account the traffic demand, is discussed in [32], where generic linear constraints were included in the transmit covariance matrix, yielding to gains compared with traditional multicolor frequency reuse schemes as large as 170%. On-board beamforming (OBBF) solutions for MIMO were discussed in [33] for multiple GW systems, also proposing potential solutions to mitigate the interbeam and interforward link interference. Guidotti and Vanelli-Coralli [34] provided a detailed system design tradeoff analysis for MMSE precoding with adaptive antennas in terms of average spectral efficiency and outage probability. Honnaiah et al. [35] proposed a traffic-driven beam design combined with user scheduling for precoding in GEO systems. The application of unsupervised machine learning techniques for scheduling in precoded GEO systems is discussed in [36]. In addition, Guidotti et al. [37] also proposed a location-based beamforming algorithm based on the knowledge of the satellite's ephemeris and the users' locations.

More recently, multicast precoding has also been addressed. Initial studies were mainly oriented toward regularized channel inversions, in which the users are served as a single terminal with an equivalent channel matrix equal to the average of the single channel matrices [38]. A pragmatic approach in which the linear precoding and ground-based beamforming are jointly optimized and computed at the ground segment is discussed in [39]. In [40], the precoding matrix is computed through a singular value decomposition. A preliminary assessment of the challenges in optimally grouping the users in multicast precoding is
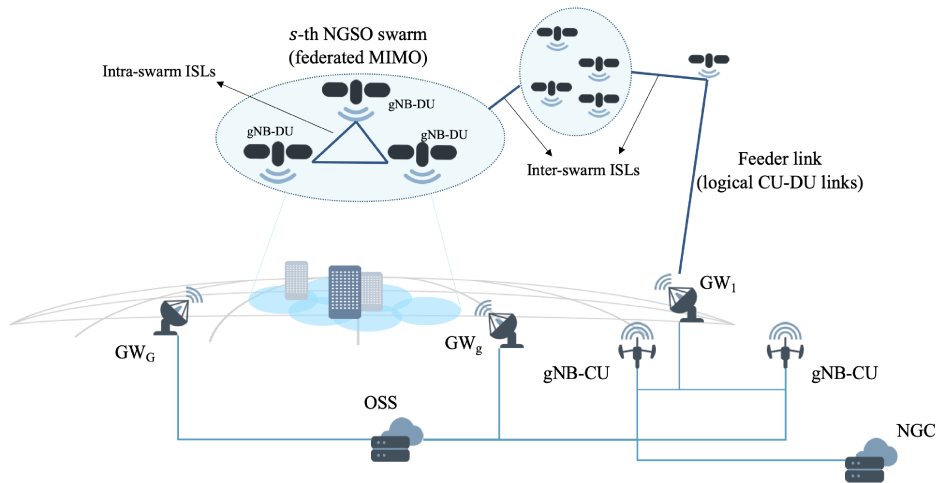
Fig. 1. System architecture for federated CF-MIMO in NGSO-based NTN with regenerative payloads, functional split, and intra/interswarm ISLs.

provided in [41], [42], [43], and [44]. In [45], a robust multigroup multicast precoding algorithm is proposed in the presence of outdated CSI. Guidotti and Vanielli-Coralli [46] proposed a thorough analysis of users grouping in multicast precoding by modeling it as a clustering problem; in addition, novel clustering algorithms, both for variable and fixed cluster sizes, are proposed showing significant performance improvements. Guidotti and Vanielli-Coralli [47] proposed a geographical scheduling for unicast and multicast precoding, based on serving together only users that belong to the same zone within the corresponding reference beam.

The application of precoding on the feeder link in the presence of multiple GWs has also been proposed, aiming at supporting high throughput services [48], [49], [50].

Recently, the authors in [51] and [52] discussed the implementation of distributed antenna array solutions in satellite communications, analyzing the array geometries to mitigate the grating lobes and introducing a novel design solution, denoted as enhanced logarithmic spiral array. Abdelsadek et al. [53] introduced the concept of satellite swarm and then focused on network/link-level handover and on a cross-layer design for power allocation and handover management; in addition, an interesting AI-based solution is also designed. In [54], the satellite swarm configuration is introduced, and then, the performance of distributed MIMO solutions is assessed on the uplink. Riera-Palou et al. [55] introduced an interesting hybrid architecture, in which CF-MIMO is implemented in the terrestrial segment, and the nonterrestrial component is used to serve users with ill-conditioned channels.

While we focus on CF-MIMO via NTN, for the sake of completeness it shall be mentioned that this technique has already emerged in the past years in the context of terrestrial systems as a ground-breaking paradigm to enhance spectral efficiency and coverage via distributed access points. Larsson et al. [56] outlined the benefits brought by the cooperation among a large number of access points to improve the spectral efficiency and interference management; in this study, the importance of efficient pilot allocation

and uplink–downlink decoupling are also discussed. In [57], practical implementation challenges are addressed considering limited backhaul, proposing a cost-effective architecture; the most important tradeoffs between performance and complexity are also discussed. Le et al. [58] focused on an interesting implementation of CF-MIMO solutions for nonorthogonal multiple access systems. Finally, Rajapaksha et al. [59] introduced data-driven solutions for the user association.

B. Article Contribution and Organization

To the best of the authors' knowledge, the extensive and valuable studies in the available literature focused on MIMO in NTN for CSI-based algorithms, with centralized architectures, i.e., all radiating elements colocated on the same satellite; moreover, architecture aspects are seldom discussed in relation to interference management techniques based on beamforming and MIMO. More specifically, in the literature, distributed antenna arrays are discussed in [51] and [52], where the authors focus on the antenna array design, in [53], focusing on power allocation and handover management, and [54], in which the swarm concept is exploited for uplink MIMO. In this work, inspired by the initial studies performed by Guidotti et al. [37] and moving from the current state-of-the-art, we:

1) propose the design of a novel location-based CF-MIMO algorithm for NTN NGSO constellations, which is completely user-centric, i.e., tailored to the users' and not based on predetermined beam lattices, and applicable in both centralized and federated architectures from multiple NTN nodes;
2) provide a unified mathematical framework for both CF (user-centric) and beam-based MIMO through federated NTN NGSO nodes;
3) design and thoroughly discuss the architecture design choices allowing the implementation of federated CF and beam-based MIMO solutions in NTN

NGSO constellations. Both regenerative, with functional split options, and transparent payloads are considered;

4) design novel power distribution approaches for federated MIMO algorithms that can be applied to swarms of NGSO nodes;

5) assess the performance taking into account different sources of nonideal knowledge at the transmitter for the computation of the beamforming matrices, including nonideal location estimation and modeling errors of the radiation pattern.

The rest of this article is organized as follows.

1) In Section II, we discuss the different architecture options and define the considered system architecture.

2) In Section III, we describe the system model and the main assumptions.

3) In Section IV, the numerical assessment is provided with both ideal and nonideal knowledge of the required information at the transmitter side, together with an extensive discussion on the recommendations and open technical challenges.

4) In Section V, we report an overview of the standardization activities related to coherent and noncoherent techniques involving multiple transmission points.

5) Finally, Section VI concludes this article.

C. Notation

Throughout this article, and if not otherwise specified, the following notations are used: bold face lower case and bold face upper case characters denote vectors and matrices, respectively. $\mathbf{a}_{i,:}$ and $\mathbf{a}_{:,i}$ denote the ith row and the ith column of matrix $\mathbf{A}$, respectively. $(\cdot)^{-1}$ denotes the matrix inversion operator. $(\cdot)^T$ denotes the matrix transposition operator. $(\cdot)^H$ denotes the matrix conjugate transposition operator. diag($\mathbf{a}$) denotes a diagonal matrix with the vector $\mathbf{a}$ on its main diagonal. $\mathbf{I}_K$ denotes the identity matrix of order K. tr($\mathbf{A}$) denotes the trace of matrix $\mathbf{A}$.

II. SYSTEM ARCHITECTURE

In this section, we provide a thorough description on the NTN architecture design to support MIMO solutions. Notably, the implementation of beamforming algorithms, detailed in Section III, is based on the knowledge of CSI or location information at the transmitter side that shall be provided by the user terminals. Different architecture options can be considered depending on where the beamforming coefficients are computed and where they are applied to the users' signals, which is defined also based on the payload capabilities. We describe in the following.

1) Section II-A describes the system architecture and the available design options.

2) In Section II-B, we discuss how they impact the beamforming algorithms due to the different signaling latencies.

3) In Section II-C, we discuss the impact of the implemented architecture on the aging of the required information at the transmitter.

4) In Section II-D, we review the functional split concepts.

A. Architecture Design Options

To support CF-MIMO in NTN, the satellite system architecture is impacted by many design choices, given in the following:

1) the type of satellite payload, i.e., regenerative or transparent;

2) the type of functional split when regenerative payloads are assumed, i.e., which layers of the NR gNB are implemented on-board in the distributed unit (gNB-DU) and which ones are implemented on-ground in the centralized unit (gNB-CU);[1]

3) the network entity in which the beamforming coefficients are computed based on the considered CF-MIMO algorithm;

4) the network entity in which the beamforming coefficients are applied to the signals, i.e., OBBF or on-ground beamforming (OGBF).

The system architecture is represented in Fig. 1 and it includes the following.

1) The ground segment, which includes G on-ground GWs providing NTN access to the terrestrial network(s). In particular, the G GWs provide the connectivity between the NGSO nodes in the constellation, the gNBs, and the next generation core network. As for the latter, the ground segment also includes the operations support systems, which is in charge of managing the overall satellite system. Depending on the type of payload on-board the NTN nodes, different elements are needed in this segment: 1) with transparent payloads, the full gNB shall be implemented on-ground and the NTN nodes basically act as relays and 2) with regenerative payloads and functional split, as shown in Fig. 1, the gNB-DUs can be located on-board, leaving the gNB-CUs on-ground. In the latter case, it shall be mentioned that each gNB-CU (full gNB with transparent payloads) can manage up to tens of connections; assuming one connection per beam, depending on the total number of beams per NTN node, multiple gNB-CUs (full gNBs) might be needed to manage all of the connections supported by the gNB-DUs (single node).

2) The nonterrestrial access segment, which includes the NGSO nodes in the constellation. We refer to nodes since the elements in the NGSO constellation

---

[1] Note that, in this article, we refer to the split definition according to 3GPP in DU and CU, as detailed in TR 38.801 [60]. Recently, a further split between the DU and a radio unit (RU) has also been used. For the sake of clarity, if not otherwise specified, we assume throughout this work that the DU also includes the RU.

TABLE I
Architecture Options for MIMO in NGSO NTN

Payload type	Architecture option			Computation	Application		Δt factors
Transparent	OGBSC	OGBF	centralized	gNB (on-ground)	gNB (on-ground)		user+feeder(+ISLs)
		OBBF			on-board		
Regenerative	OGBSC	OGBF	federated or centralized	gNB-CU (on-ground)	gNB-CU (on-ground)		user+feeder(+ISLs)
		OBBF			gNB-DU (on-board)		
	OBBSC	OBBF		gNB-DU (on-board)	gNB-DU (on-board)		user(+ISLs)[1]

Note 1: The ISLs with OBBSC solutions are intraswarm and, thus, might be negligible in terms of additional latency.

can be any type of platform on one or more NGSO orbits, e.g., LEO satellites organized in one or more subconstellations at different altitudes, or a high altitude platform stations formation. As mentioned above, these nodes can implement either a transparent or a regenerative payload, depending on the cost and complexity of the target system. With respect to coverage, in 3GPP beam-based coverage solutions we might have: 1) Earth-fixed beams, i.e., through digitally steering of the signals, the coverage area generated by each node is fixed on-ground independently of its position on the orbit (as long as it falls in the node field of view) or 2) Earth-moving beams, i.e., the coverage area of each node is always centered around its subnode point and, thus, the beams move on-ground along with the node on its orbit. When CF approaches are considered, the very concept of beams is not necessary anymore, as extensively discussed in Section III.

3) The on-ground user segment, composed by a potentially massive number of user equipments (UEs), either fixed or moving. These directly connect to the serving node(s) by means of the Uu air interface through the user access link. In this work, we consider both handheld terminals and very small aperture terminals (VSAT).

Based on the above observations, the selected functional split option [60] has an impact on where the users' scheduling and beamforming coefficients are computed; in particular, two architecture design options are possible: 1) on-ground beamforming and scheduling computation (OGBSC), where the scheduling and coefficients computation is performed at the on-ground gNB-CU or 2) on-board beamforming and scheduling computation (OBBSC), where these operations are performed at the on-board gNB-DUs. Moreover, NGSO-based systems with regenerative payloads allow the implementation of federated (distributed) MIMO solutions, in which multiple satellites cooperate to implement MIMO transmissions. We refer to the cooperating satellites as satellite swarm or swarm.

B. Centralized and Federated MIMO

Table I summarizes the architecture options based on the payload type, where the users' scheduling and beamforming coefficients are computed (OGBSC or OBBSC), where the beamforming coefficients are applied to the users' signals

(OGBF or OBBF), and whether a federated MIMO solution is possible or not. Depending on the selected option, the entity performing the different operations can be identified.

With legacy transparent payloads, scheduling and beamforming are entirely defined on-ground (OGBSC); then, the beamforming coefficients can be applied to the users' signals either on-board (OBBF) or on-ground (OGBF). In this scenario, no federated solution is possible and each satellite in the constellation operates as a standalone node; in fact, federated MIMO architectures require a tight time and frequency synchronization among the cooperating satellites in the swarm, which can only be achieved by means of intraswarm intersatellite links (ISLs) with regenerative payloads.

When considering future regenerative payloads, legacy centralized architectures are clearly still possible. However, the exploitation of the advanced on-board computational capabilities supports two additional MIMO architecture options: 1) OBBSC, in which the users' scheduling and beamforming coefficients are computed on-board and 2) federated MIMO, in which multiple satellites can tightly synchronize to realize a distributed MIMO system. OBBSC solutions allow to perform all operations at the on-board gNB-DU: 1) computation of the users' scheduling and beamforming coefficients and 2) application of the beamforming coefficients to the users' signals. Such advanced capabilities allow to implement either a centralized or a federated MIMO algorithm. In the former case, each satellite in the NGSO constellation can operate as a standalone NTN node, thus leading to a centralized architecture; all of the UEs in the satellite's service area send the required ancillary information for the considered MIMO algorithm (CSI or location, as discussed in Section III) on the return link and the satellite implements a centralized MIMO algorithm. With federated MIMO, the synchronization and coordination among multiple NTN nodes in a single swarm is possible. In particular, the following holds.

1) A master gNB-DU collects the ancillary information (CSI or location) from the UEs, either directly or with the support of intraswarm ISLs.
2) The master gNB-DU computes the users' scheduling and beamforming coefficients and sends the beamformed signals to the other satellites in the swarm.
3) Thanks to the intraswarm ISLs, the satellites in the swarm can tightly synchronize the transmission of the beamformed signals in the time and frequency
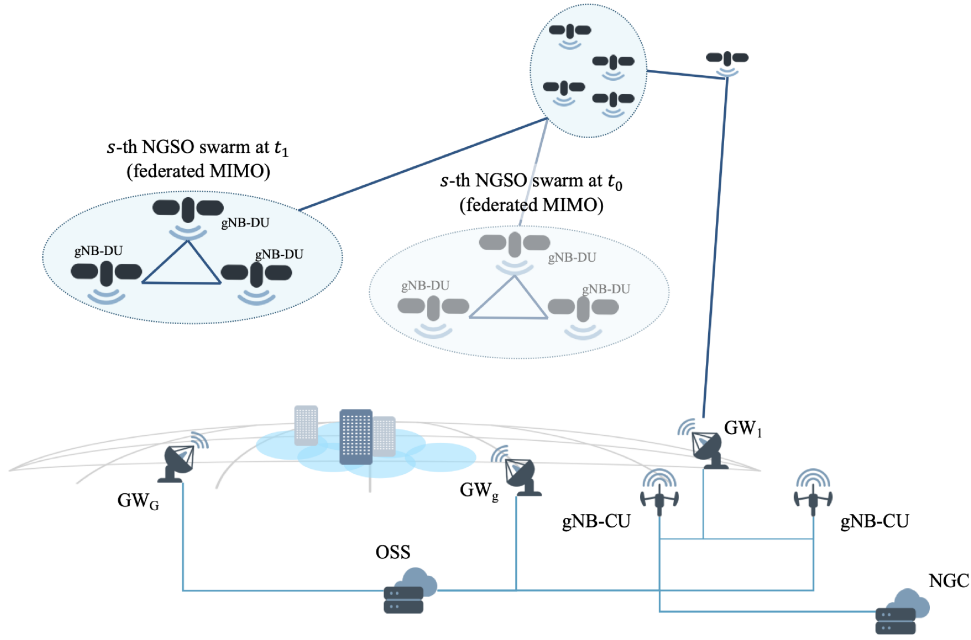
Fig. 2. System architecture for federated CF-MIMO in NGSO-based NTN: estimation and transmission phases.

domains, leading federated MIMO via a distributed antenna system.

It is worthwhile highlighting that federated MIMO is also possible with the on-ground computation of the users' scheduling and beamforming coefficients provided by OG-BSC architectures; in this case, the NGSO satellites in the swarm still realize a tightly synchronized distributed antenna system, with the only difference being that the ancillary information from the UEs is sent to the on-ground gNB-CU, which is in charge of all computations. Then, the beamforming coefficients can be applied either on-ground (OGBF) or on-board (OBBF).

On the one hand, the implementation of federated MIMO is challenging in terms of increased system complexity, due to the need for regenerative payloads with advanced on-board processors (OBP) and tight intraswarm synchronization via ISLs. On the other hand, the deployment of a flying distributed antenna system allows to tackle the detrimental impact of harsh propagation environments, thanks to the spatial diversity at the transmitter.

C. Ancillary Information Aging: OGBSC and OBBSC

The choice between OGBSC and OBBSC is fundamental for MIMO in NTN. In fact, the MIMO algorithms considered in this work (described in Section III) require either the CSI vectors or the location estimated at the UEs' locations to build the beamforming matrix, denoted as ancillary information. The ancillary information is obtained by the UEs at an estimation time instant t_0 and then sent to the network element computing the coefficients: the on-ground gNB-CU with OGBSC or the master on-board gNB-CU with OBBSC. The transmission of the beamformed signals from either the federated gNB-CUs

or the standalone gNB-CU (centralized architectures) then happens at a transmission time instant $t_1 > t_0$. During the aging interval $\Delta t = t_1 - t_0$, both the NGSO nodes and the UEs have moved and; thus, there is a misalignment between the actual channel encountered during the transmission and the ancillary information used to compute the beamforming matrix. This is represented in Fig. 2, where only the swarm movement is depicted for the sake of clarity. Notably, the MIMO performance is deeply impacted by any misalignment between the actual channel and the beamforming matrix; thus, the smaller the aging interval, the better the performance of federated MIMO.

When considering OGBSC, the users' scheduling and coefficients are computed on-ground and, thus, the aging interval can be computed as

$$\Delta t_{\mathrm{OGBSC}} = \tau_{\mathrm{user}} + \tau_{\mathrm{feeder}}^{(\mathrm{DL})} + \tau_{\mathrm{feeder}}^{(\mathrm{UL})} + \tau_p + \tau_{\mathrm{rout}} + \tau_{\mathrm{ad}} \quad (1)$$

where the following holds.

1) τ_{user} is the latency on the user return link.
2) $\tau_{\mathrm{feeder}}^{(\mathrm{DL})}$ is the latency on the feeder downlink.
3) $\tau_{\mathrm{feeder}}^{(\mathrm{UL})}$ is the latency on the feeder uplink.
4) τ_p is the processing delay to compute the users' scheduling and beamforming coefficients.
5) τ_{rout} is the latency due to routing on the ISLs, if present.
6) τ_{ad} includes any additional source of latency.

When OBSBC is considered, the aging interval is significantly reduced; in fact, all computations are performed on-board, and thus

$$\Delta t_{\mathrm{OBBSC}} = \tau_{\mathrm{user}} + \tau_p + \tau_{\mathrm{ad}}. \quad (2)$$

Compared with $\Delta t_{\mathrm{OGBSC}}$, $\Delta t_{\mathrm{OBBSC}}$ only includes the over-the-air latency on the user access link, in addition to the
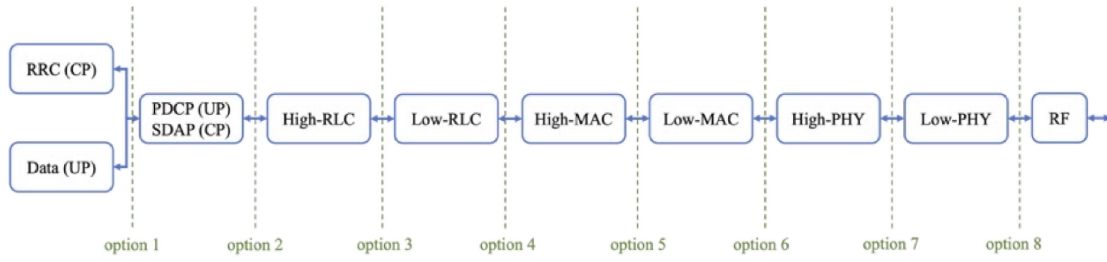
Fig. 3. Functional split options as per 3GPP TR 38.801.

processing and additional delays. Clearly, this advantage is lost if the functional split option does not allow to perform the required computations on-board, i.e., regenerative payloads with an OGBSC approach. The factors impacting the aging interval Δt are summarized in Table I.

It is worthwhile highlighting that the advantage of OBBSC is not only related to the reduction of the aging interval and, thus, improving the MIMO performance; in fact, the signaling overhead on the feeder link, and on any interswarm ISL that might be needed to connect the swarm with the serving gNB-CU, is massively reduced. The reduction in signaling also includes all information that is needed to implement the desired RRM algorithm, which might include the UEs' capacity request and type of traffic, as well as the terminal class. With respect to the latter, it shall be mentioned that this information might be classified by the manufacturers; in this case, an estimate can be identified based on ancillary terminal parameters/information. RRM aspects are not addressed in this work, without impacting the generality of the proposed architectures or algorithms. Finally, it is worthwhile highlighting that both the above advantages are achieved with both centralized and federated MIMO architectures.

D. Functional Split Options

To conclude the analysis on the architecture options, we now briefly summarize the available functional split solutions discussed in 3GPP specifications. In the initial study phase for the definition of the 5G standard, eight functional split options were identified, as shown in Fig. 3 [60]. In the normative phase, 3GPP reached the consensus to implement functional split option 2, i.e., implementing up to the radio link control layer in the DU and all higher layers in the CU [61], and the DU and CU are connected through the logical F1 interface. Other split options are possible, but they are not fully compliant with 3GPP and require the implementation of open radio access network (O-RAN) or enhanced common public radio interface solutions.

In the 3GPP specifications, scheduling of both uplink and downlink transmissions is defined and performed at medium access control layer in the gNB. To perform such operation, the gNB gathers all the required measurements from the served UEs and, based on the implemented proprietary scheduling algorithm, allocates the resources to the users. To ease the system complexity, and reduce the

signaling overhead, we can assume that the network element implementing the scheduler also computes the beamforming matrix; this is in line with the architectures introduced in this work, in which both operations are performed on-ground (OGBSC) or on-board (OBBSC). Referring to Table I, and taking these considerations into account, we can observe that: 1) both OGBSC architectures with regenerative payloads are compliant with option 2, with scheduling and beamforming computed in the gNB-CU and 2) the OBBSC architecture with on-board computation requires the implementation of functional split option 4 (or lower), thus requiring O-RAN capabilities.

III. SYSTEM MODEL

We consider a constellation with M NGSO nodes providing connectivity to the on-ground UEs in the service area. Notably, for a generic coverage area, only a subset of nodes will be visible from all of the UEs, based on the nodes' field of view and on minimum elevation angle requirements. In the following, we assume that a single swarm of N_{node} nodes is visible from all of the N_{ue} UEs in the considered area. Each node is equipped with a uniform planar array (UPA) with N_F radiating elements; for the sake of simplicity, and without affecting the generality of our work, we assume that all of the nodes are at the same altitude and equipped with the same antenna configuration (i.e., number of radiating elements, UPA configuration, and element radiation pattern).

A. Channel

As discussed in Section II-C, the users estimate the ancillary information required for the considered MIMO algorithm (CSI or location) at the estimation time instant t_0; then, the actual transmission of the beamformed signals occurs at the transmission time instant t_1. During the aging interval, there are several sources of misalignment between the actual channel at t_1 and the beamforming matrix based on information obtained at t_0, given in the following:

1) the nodes moved along their orbits;
2) the UEs might have moved, depending on the terminal type;
3) different realizations of the stochastic terms in the channel coefficients (e.g., large scale losses, scintillation) are present.

As for the latter, the channel coefficient between the ith on-ground UE and the nth radiating element of the UPA on-board the sth node at the generic time instant t can be computed as [41], [42], [44], [47]

$$h_{i,n,s}^{(t)} = \frac{g_{i,n,s}^{(TX,t)} g_{i,n,s}^{(RX,t)}}{4\pi \frac{d_{i,s}^{(t)}}{\lambda} \sqrt{L_{i,s}^{(t)} \kappa B T_i}} e^{-J\frac{2\pi}{\lambda} d_{i,s}^{(t)}} e^{-J\varphi_{i,s}^{(t)}} \quad (3)$$

where the following holds.

1) $d_{i,s}^{(t)}$ is the slant range between the ith user and the sth node, which is assumed to be the same for all the colocated radiating elements on-board the node.
2) λ is the signal wavelength.
3) $\kappa B T_i$ denotes the thermal noise power, with B being the user bandwidth (for simplicity assumed to be the same for all users), and T_i the equivalent noise temperature of the ith receiver.
4) $L_{i,s}^{(t)}$ represents the additional losses between the sth node and the ith user, assumed to be the same for all the colocated radiating elements on-board the node.
5) $g_{i,n,s}^{(TX,t)}$ and $g_{i,n,s}^{(RX,t)}$ represent the transmitting and receiving complex antenna patterns between the ith user and the nth radiating element on-board the sth node, respectively.
6) $\varphi_{i,s}^{(t)}$ is the phase misalignment that might be present between different nodes due to nonideal swarm synchronization, modeled as a uniform random variable (r.v.) $\mathcal{U}(0, 2\pi)$.

The additional losses are computed based on TR 38.811 [62]

$$L_{i,s}^{(t)} = L_{i,s}^{(SHA,t)} + L_{i,s}^{(ATM,t)} + L_{i,s}^{(SCI,t)} + L_{i,s}^{(CL,t)} \quad (4)$$

in which the following holds.

1) $L_{i,s}^{(SHA,t)}$ denotes the log-normal shadowing loss with standard deviation σ_{SHA}.
2) $L_{i,s}^{(ATM,t)}$ includes the atmospheric loss due to gaseous absorption.
3) $L_{i,s}^{(SCI,t)}$ is the scintillation loss.
4) $L_{i,s}^{(CL,t)}$ is the clutter loss (CL), to be included for UEs in nonline-of-sight (NLOS) conditions.

Referring to the 3GPP channel model, the UE is defined to be in LOS or NLOS conditions with a probability that is a function of the elevation angle and the propagation environment (suburban, urban, and dense urban). In this context, we assume that a UE that is LOS (NLOS) conditions during the estimation phase is still in LOS (NLOS) conditions in the transmission phase. This assumption is motivated by observing that the probability that the propagation conditions of the UE will change from LOS (NLOS) to NLOS (LOS) after a few ms is negligible; in fact, the values of the differential elevation angle between t_0 and t_1 are negligible[2] (within $\pm 0.01°$), considering that the probabilities of LOS or NLOS conditions are provided with a $10°$ granularity in TR 38.811 [62]. This assumption implies that the UE has the same CL and σ_{SHA} in both the estimation and transmission phases, but the realizations of the log-normal r.v. modeling the shadowing are different.

B. Received Signal

In the following, the estimated CSI vector between the sth node and the ith user is represented by $\mathbf{h}_{i,s}^{(t_0)} = [h_{i,1,s}^{(t_0)}, \ldots, h_{i,N_F,s}^{(t_0)}]$. For the generic ith user, its overall channel signature can be obtained by collecting the CSI vectors from all of the NGSO nodes into the $N_{node}N_F$-dimensional $\mathbf{h}_{i,:}^{(t_0)} = [\mathbf{h}_{i,1}^{(t_0)}, \ldots, \mathbf{h}_{i,N_{node}}^{(t_0)}]$. Finally, the overall $N_{ue} \times (N_{node}N_F)$ channel matrix at the estimation time t_0 is given by $\mathbf{H}_{sys}^{(t_0)} = [(\mathbf{h}_{1,:}^{(t_0)})^T, \ldots, (\mathbf{h}_{N_{node},:}^{(t_0)})^T]^T$. For each time slot, the RRM scheduling function $\mathcal{S}$ provides a subset of K users to be served, leading to a $K \times (N_{node}N_F)$ channel matrix $\mathbf{H}^{(t_0)} = \mathcal{S}(\mathbf{H}_{sys}^{(t_0)}) \subseteq \mathbf{H}_{sys}^{(t_0)}$. Based on the channel matrix estimated at t_0, the beamforming algorithm (detailed in the next sections) provides a $(N_{node}N_F) \times K$ complex beamforming matrix $\mathbf{W}^{(t_0)} = \mathcal{B}(\mathbf{H}^{(t_0)})$, which projects the K-dimensional column vector $\mathbf{s} = [s_1, \ldots, s_{N_{ue}}]^T$ containing the unit-variance user symbols into the $(N_{node}N_F)$-dimensional space defined by all of the swarm radiating elements. The signal received by the generic kth UE in FFR, with $k = 1, \ldots, K$, is given by[3]

$$y_k = \underbrace{\mathbf{h}_{k,:}^{(t_1)} \mathbf{w}_{:,k}^{(t_0)} s_k}_{\text{intended}} + \underbrace{\sum_{\substack{\ell=1 \\ \ell \neq k}}^{K} \mathbf{h}_{k,:}^{(t_1)} \mathbf{w}_{:,\ell}^{(t_0)} s_\ell}_{\text{interfering}} + z_k \quad (5)$$

where z_k is a circularly symmetric Gaussian r.v. with zero mean and unit variance, which is licit observing that the channel coefficients in (3) are normalized to the noise power. From (5), the K-dimensional vector of received symbols is

$$\mathbf{y} = \mathbf{H}^{(t_1)} \mathbf{W}^{(t_0)} \mathbf{s} + \mathbf{z}. \quad (6)$$

As previously discussed, it can be noticed that there is a misalignment between the estimated channel matrix exploited to compute $\mathbf{W}^{(t_0)}$, function of $\mathbf{H}^{(t_0)}$, and the actual channel in the transmission phase, $\mathbf{H}^{(t_1)}$.

The signal-to-interference-plus-noise ratio (SINR) of the generic kth UE can be obtained as

$$\gamma_k = \frac{\left| \mathbf{h}_{k,:}^{(t_1)} \mathbf{w}_{:,k}^{(t_0)} \right|^2}{1 + \sum_{\substack{\ell=1 \\ \ell \neq k}}^{K} \left| \mathbf{h}_{k,:}^{(t_1)} \mathbf{w}_{:,\ell}^{(t_0)} \right|^2}. \quad (7)$$

From the above SINR, the rate achieved by the kth user can be evaluated either from the Shannon bound formula or from the adopted modulation and coding scheme (MCS). In this framework, 3GPP TR 38.803 reports that the spectral efficiency for system-level simulations can be obtained through

---

[2]These results were obtained with $N_{node} = 2$ and the system configuration described in Section IV.

[3]We are using k as the user index instead of i to distinguish between the overall channel matrix, $\mathbf{H}_{sys}^{(t_0)}$, and that of the scheduled users only, $\mathbf{H}^{(t_0)}$.

the following truncated form of the Shannon bound [63]:

$$\eta_k = \begin{cases} 0, & \gamma_k < \gamma_{\min} \\ \varepsilon \cdot \log_2\left(1 + \gamma_k\right), & \gamma_{\min} \leq \gamma_k < \gamma_{\max} \\ \varepsilon \cdot \log_2\left(1 + \gamma_{\max}\right), & \gamma_k \geq \gamma_{\max} \end{cases} \tag{8}$$

where $\gamma_{\min} = -10$ dB and $\gamma_{\max} = 30$ dB are the minimum and maximum SINR of the MCS, respectively, and ε is an attenuation factor representing the implementation loss. Since the attenuation factor is a multiplicative term outside of the Shannon formula, in the following, we assume $\varepsilon = 1$ since a different value only acts as a scaling factor on all of the results discussed below, i.e., it does not impact the relationship among the different techniques and scenarios and the general trends.

C. CSI-based CF-MIMO

CSI-based techniques require each UE to estimate the CSI vector $\mathbf{h}_{k,:}^{(t_0)}$ during the estimation phase and to report it to the network element in charge of the computation of $\mathbf{W}^{(t_0)}$ (i.e., on-ground gNB-CU with OGBSC or master on-board gNB-DU with OBBSC). Notably, among these, MMSE beamforming is the best algorithm in the sense of SINR maximization; as such, it is considered as the upper-bound performance benchmark[4]

$$\mathbf{W}_{\mathrm{MMSE}}^{(t_0)} = \mathbf{H}^H \left(\mathbf{H}\mathbf{H}^H + \mathrm{diag}(\boldsymbol{\alpha})I_K\right)^{-1} \tag{9}$$

where, for the sake of clarity, we dropped the time instant t_0 from the channel matrix. In the above equation, $\mathrm{diag}(\boldsymbol{\alpha})$ is a vector of K regularization factors; since the channel coefficients are normalized to the noise power, the optimal value is given by $\boldsymbol{\alpha} = \mathbf{1}_K N_F / P_t$, where P_t is the available power per node in the swarm, and $\mathbf{1}_K$ is an all-ones K-dimensional vector [65].

D. Location-Based CF-MIMO

Inspired by the spatially sampled (SS-MMSE) algorithm proposed by Guidotii et al. [37] in a previous work, we design a new location-based CF-MIMO solution. In particular, when the UEs are equipped with global navigation satellite system (GNSS) capabilities, they can estimate their locations and provide them to the gNB-CU (OGBSC) or gNB-DU (OBBSC). This information, combined with the knowledge of the swarm ephemeris, can be exploited to infer the channel coefficients between the UE and the NGSO nodes. In particular, all terms in (3) can be estimated, exception made for the additional losses and the phase misalignment, which are stochastic terms

$$\widetilde{h}_{k,n,s}^{(t)} = \frac{\widetilde{g}_{k,n,s}^{(TX,t)} \widetilde{g}_{k,n,s}^{(RX,t)}}{4\pi \frac{\widetilde{d}_{k,s}^{(t)}}{\lambda} \sqrt{\kappa B T_k}} e^{-j\frac{2\pi}{\lambda}\widetilde{d}_{k,s}^{(t)}} \tag{10}$$

where the tilde denotes that the terms are actually deduced from the relative positions of the UE and the swarm nodes.

Clearly, the accuracy of the estimated channel coefficient is directly impacted by the accuracy of the location estimate performed by the UE and by the accuracy of the ephemeris data. In addition, as extensively discussed in Section IV-D, $\widetilde{g}_{k,n,s}^{(TX,t)}$ and $\widetilde{g}_{k,n,s}^{(RX,t)}$ might also be impacted by a nonideal knowledge of the radiation pattern, i.e., the antenna mathematical model used to compute the antenna pattern might not be flawlessly representing the actual radiation. From (10), we can compute the beamforming matrix for the proposed location-based MMSE (LB-MMSE) as

$$\mathbf{W}_{\mathrm{LB-MMSE}}^{(t_0)} = \widetilde{\mathbf{H}}^H \left(\widetilde{\mathbf{H}}\widetilde{\mathbf{H}}^H + \mathrm{diag}(\boldsymbol{\alpha})\mathbf{I}_K\right)^{-1}. \tag{11}$$

Compared with CSI-based techniques, LB-MMSE has the advantage of not requiring the UEs to estimate the channel coefficients, with manifold benefits. First, the signaling overhead is significantly reduced, as the CSI vectors are not needed at the gNB-CU (OGBSC) or gNB-DU (OBBSC) and the UEs' positions require much smaller data packets to be transmitted.[5] Moreover, it shall be noticed that the estimation of the channel coefficients is typically assuming the presence of beams, each of which is associated with a known data/pilot sequence on which the estimation is performed; when moving to CF solutions, the concept of beam is lost and, thus, adjustments to the air interfaces would be needed. Finally, this approach also avoids the well-known issue of estimating the channel coefficients in low signal-to-interference ratio (SIR) conditions. In fact, some of the known data/pilot sequences might be received with a significantly lower power compared with others. In such conditions, the UE is not able to estimate the channel coefficient, which shall then be either inferred at the gNB-CU/gNB-DU through more complex approaches, e.g., machine learning, or reported as a null in the channel matrix, which might lead to sparse ill-conditioned matrices.

E. Beam-Based MIMO

Aiming at providing a complete performance comparison for the newly designed LB-MMSE algorithm, we also consider two beam-based solutions. The first one is a system implementing a phase-only digital beam steering. In this case, an on-ground hexagonal beam lattice is defined based on the desired number of tiers around the center of the coverage area and on the 3-dB angular beamwidth, $\vartheta_{3\mathrm{dB}}$, as defined in TR 38.821 [66]. Denoting as $\mathbf{c}_{\ell,s}$ the (u, v) coordinates of the generic ℓth beam center from the sth node,[6] its nth beamforming coefficient is

$$b_{n,\ell,s} = \frac{1}{\sqrt{N_F}} e^{-jk_0 \mathbf{r}_{n,s} \cdot \mathbf{c}_{\ell,s}} \tag{12}$$

where $k_0 = 2\pi / \lambda$ is the wave number, and $\mathbf{r}_{n,s}$ is the position of the nth radiating element on the sth on-board UPA.

---

[4]This is an equivalent and more computationally efficient formulation of the MMSE beamformer [64].

[5]Assuming 32 b for floating point values, 64 b are needed per channel coefficient per user; this leads to $64 \cdot N_F$ b per user. For the location, each coordinate in the global positioning system requires 24 b, leading to 48 b per user.

[6]The (u, v) system is centered at the satellite and, thus, the coordinates depend on the considered node [64].

TABLE II
Summary of the Considered Beamforming Algorithms

Algorithm	Channel coefficient	Beamforming matrix	Information	Errors
MMSE	$h_{k,n,s}^{(t)} = \dfrac{g_{k,n,s}^{(TX,t)} g_{k,n,s}^{(RX,t)}}{4\pi \frac{d_{k,s}^{(t)}}{\lambda} \sqrt{L_{k,s}^{(t)} \kappa B T_k}} e^{-\jmath \frac{2\pi}{\lambda} d_{k,s}^{(t)}} e^{-\jmath \varphi_{k,s}^{(t)}}$	$\mathbf{H}^H \left(\mathbf{H}\mathbf{H}^H + \text{diag}(\boldsymbol{\alpha})\mathbf{I}_K\right)^{-1}$	CSI	CSI estimation Low-SINR estimation Air interface adj. UE/node movement
LB-MMSE	$\widetilde{h}_{k,n,s}^{(t)} = \dfrac{\widetilde{g}_{k,n,s}^{(TX,t)} \widetilde{g}_{k,n,s}^{(RX,t)}}{4\pi \frac{\widetilde{d}_{k,s}^{(t)}}{\lambda} \sqrt{\kappa B T_k}} e^{-\jmath \frac{2\pi}{\lambda} \widetilde{d}_{k,s}^{(t)}}$	$\widetilde{\mathbf{H}}^H \left(\widetilde{\mathbf{H}}\widetilde{\mathbf{H}}^H + \text{diag}(\boldsymbol{\alpha})\mathbf{I}_K\right)^{-1}$	Location	Location estimation Radiation pattern model UE/node movement
SS-MMSE	$\widetilde{h}_{k,n,s}^{(BC,t)} = \dfrac{\widetilde{g}_{k,n,s}^{(BC,TX,t)} \widetilde{g}_{k,n,s}^{(BC,RX,t)}}{4\pi \frac{\widetilde{d}_{k,s}^{(BC,t)}}{\lambda} \sqrt{\kappa B T_k}} e^{-\jmath \frac{2\pi}{\lambda} \widetilde{d}_{BC,k,s}^{(t)}}$	$\widetilde{\mathbf{H}}_{BC}^H \left(\widetilde{\mathbf{H}}_{BC} \widetilde{\mathbf{H}}_{BC}^H + \text{diag}(\boldsymbol{\alpha})\mathbf{I}_K\right)^{-1}$	Location	Location estimation Radiation pattern model Approx. location UE/node movement
MB	$b_{n,\ell} = \frac{1}{\sqrt{N_F}} e^{-\jmath k_0 \mathbf{r}_n \cdot \mathbf{c}_\ell}$	$\left[b_{n,\ell}\right]_{\substack{n=1,\dots,N_F \\ \ell=1,\dots,N_B}}$	Location	Location estimation Approx. location UE/node movement

Assuming that in each time slot one user per beam is served, the beamforming matrix of the sth node is fixed and it is given by $\mathbf{W}_{PO,s} = [b_{n,\ell,s}]_{\substack{n=1,\dots,N_F \\ \ell=1,\dots,N_B}}$, where N_B is the number of beams. The overall $(N_{\text{node}}N_F) \times N_B$ beamforming matrix $\mathbf{W}_{PO}$ is obtained by vertically concatenating the $N_F \times N_B$ $\mathbf{W}_{PO,s}$, $s = 1, \dots, N_{\text{node}}$, node matrices. It shall be noticed that, when advanced scheduling algorithms are implemented and not all of the beams are illuminated in all time slots, the switchable MB MIMO algorithm proposed in the literature [64] is obtained. In the following, we refer to MB beamforming also with all beams being illuminated.

The second beam-based approach is the SS-MMSE algorithm [37]. In this case, the generic ith user is associated with the closest beam center, thus leading to a beam-based solution; then, the channel coefficients are estimated based on (10), in which each term is computed based on the corresponding beam center location, and not the estimated UE location

$$\widetilde{h}_{i,n,s}^{(BC,t)} = \frac{\widetilde{g}_{i,n,s}^{(BC,TX,t)} \widetilde{g}_{i,n,s}^{(BC,RX,t)}}{4\pi \frac{\widetilde{d}_{i,s}^{(BC,t)}}{\lambda} \sqrt{\kappa B T_i}} e^{-\jmath \frac{2\pi}{\lambda} \widetilde{d}_{BC,i,s}^{(t)}} \qquad (13)$$

where BC indicates that the terms shall be computed at the corresponding beam center. From this estimated channel matrix, the MMSE equation is again applied to obtain $\mathbf{W}_{\text{SS-MMSE}}$. Thus, this approach is different from LB-MMSE since it is beam-based and it approximates the UEs' locations to those of closest beam centers.

Table II summarizes the different beamforming techniques, reporting the required information, the beamforming and channel coefficient equations, and the potential sources of misalignment between the channel matrices at t_0 and t_1. It shall be noticed that, for SS-MMSE, $\widetilde{\mathbf{H}}_{BC}$ denotes the beam centers channel matrix estimated based on (13).

F. Power Distribution: Centralized CF-MIMO

The normalization of the beamforming matrix is a fundamental operation, since it determines how the on-board available power is redistributed and emitted through the radiating elements cooperating in the definition of the beamforming scheme [34], [37]. In fact, the Frobenius norm of the beamforming matrix, $\|\mathbf{W}\|_F^2$, represents the total emitted power and, by applying the MMSE formula, there is no guarantee that such power will be upper bounded so as to not exceed the total available power. First, considering a single node in the swarm, for the sake of simplicity, this means that there might be situations in which $\|\mathbf{W}\|_F^2 > P_t$, where P_t denotes the total available power on-board. Aiming at addressing this issue, following normalizations have been considered in the literature.

1) *Sum power constraint (SPC):*

$$\widetilde{\mathbf{W}} = \sqrt{\frac{P_t}{\|\mathbf{W}\|_F^2}}\mathbf{W} = \sqrt{\frac{P_t}{\text{tr}\left(\mathbf{W}\mathbf{W}^H\right)}}\mathbf{W}. \qquad (14)$$

This normalization guarantees that: 1) the overall power allocated by the beamforming matrix is equal to that actually available, i.e., $\|\mathbf{W}\|_F^2 = P_t$ and 2) preserves the orthogonality among the beamforming matrix columns, i.e., it does not disrupt the optimal MMSE solution since all columns are normalized by the same scalar quantity. However, SPC does not control the power emitted per radiating element, which might lead to a performance degradation due to driving the on-board high power amplifiers (HPAs) close to or above the saturation level, thus introducing undesired nonlinear effects.

2) *Maximum power constraint (MPC):*

$$\widetilde{\mathbf{W}} = \sqrt{\frac{P_t}{K \max_{k=1,\dots,K} \left\|\mathbf{w}_{:,k}\right\|^2}}\mathbf{W}. \qquad (15)$$

In this case, the normalization is similar to SPC, with the only difference being that only one radiating element is emitting the maximum allowed power, while all of the others emit a lower power level. Thus, the following holds.

   a) The overall emitted power is below the available power, i.e., $\|\mathbf{W}\|_F^2 < P_t$.

   b) The orthogonality among the beamforming matrix columns is preserved.

   c) The emitted power is limited per radiating element.

     However, since only one radiating element is emitting the maximum power, while the others are significantly limited in their emissions, this approach might lead to a degradation of

the SNR and, in general, to a performance loss.

3) *Per antenna constraint (PAC):*

$$\widetilde{\mathbf{W}} = \sqrt{\frac{P_t}{K}} \text{diag}\left(\frac{1}{\|\mathbf{w}_{1,:}\|}, \ldots, \frac{1}{\|\mathbf{w}_{K,:}\|}\right)\mathbf{W}. \quad (16)$$

With this approach, each radiating element transmits at an equal power level, thus ensuring that the overall available power is not exceeded, i.e., $\|\mathbf{W}\|_F^2 = P_t$. However, since each row of the beamforming matrix is normalized independently from each other, the orthogonality of the beamformer columns are disrupted and potentially large performance degradation is introduced.

G. Power Distribution: Federated CF-MIMO

When multiple NGSO nodes are considered, some further considerations are needed. In this case, the beamforming matrix includes the power emitted by radiating elements on-board different nodes. Consequently, the normalizations shall be adjusted to satisfy the power constraints per node. Assuming that each node has the same available on-board power, $P_{t,\text{node}}$, we introduce the following normalizations.

1) *Swarm SPC (sSPC):* Directly applying the SPC normalization with a total power $N_{\text{node}}P_{t,\text{node}}$ guarantees that this power is not exceeded at swarm level, i.e., $\|\mathbf{W}\|_F^2 = N_{\text{node}}P_{t,\text{node}}$; however, a single node might be required to emit more power than available. To circumvent this issue, the swarm-based sSPC normalization is introduced based on the observation that the overall $(N_{\text{node}}N_F) \times K$ beamforming matrix can be divided in blocks corresponding to the single-nodes beamforming matrices, i.e.

$$\mathbf{W} = \begin{bmatrix} \mathbf{W}_1 \\ \vdots \\ \mathbf{W}_{N_{\text{node}}} \end{bmatrix} \quad (17)$$

with $\mathbf{W}_s$ denoting the $N_F \times K$ beamforming matrix of the sth NGSO node. Each node beamforming matrix can be normalized with the SPC approach as a standalone matrix, guaranteeing that: 1) the overall emitted power satisfies $\|\mathbf{W}\|_F^2 = N_{\text{node}}P_{t,\text{node}}$ and 2) each satellite emits a power $\|\mathbf{W}_s\|_F^2 = P_{t,\text{node}}$, $s = 1, \ldots, N_{\text{node}}$. Clearly, this approach leads to a slight degradation in the performance, because a normalization that is not scalar for the entire beamforming matrix $\mathbf{W}$ leads to a loss of orthogonality in the beamforming matrix columns, i.e., to a loss in its interference cancellation capabilities.

2) *Swarm MPC (sMPC):* In this case, there are two options. In fact, if the objective is to preserve the orthogonality in the beamforming matrix columns, then (15) can be directly applied since only one radiating element will emit its maximum power; this guarantees the preservation of the orthogonality, but

actually leads to lower emitted power levels, since only a single element from a single node in the swarm will transmit the maximum power. Another possibility is to better exploit the available power, by normalizing with the MPC approach each node matrix, as in the sSPC solution; this guarantees that the overall emitted power is still satisfying the condition $\|\mathbf{W}\|_F^2 < N_{\text{node}}P_{t,\text{node}}$ and that each node emits a power $\|\mathbf{W}_s\|_F^2 < P_{t,\text{node}}$, $s = 1, \ldots, N_{\text{node}}$. Only a single element per node emits its maximum power. In the following, we assume the latter solution is implemented.

As for PAC, from (16) it can be noticed that no issue arises since each row of the beamforming matrix is individually normalized to guarantee that each radiating element emits the same power level. Thus, as previously discussed, we are ensuring that each nodes emits a total power $P_{t,\text{node}}$ and that the swarm collectively emits a power $N_{\text{node}}P_{t,\text{node}}$, with a performance loss related to the disrupted orthogonality in the beamforming matrix columns on a node basis.

In the following, we consider the (s)SPC and (s)MPC normalizations. It was observed that, as expected, the PAC approach has a poor interference cancellation performance and, as such, it usually leads to very low SINRs. The (s)MPC solution is a viable normalization approach since it satisfies all power constraints and avoids operating the on-board HPAs in the nonlinear region. The (s)SPC normalization is retained as it provides an upper bound performance, even though not practically implementable due to the possibility that a node is required to transmit more power than available. The network element performing the power normalization is that in which the beamforming matrix coefficients are computed, which depends on the selected architecture. Thus, as discussed in Section II-D, with OGBSC the power distribution is defined in the gNB-CU, while with OBBSC it is computed in the on-board gNB-DU.

IV. NUMERICAL ASSESSMENT

In this section, we discuss the extensive numerical results obtained through Monte Carlo simulations with the MMSE, LB-MMSE, SS-MMSE, and MB algorithms. The system configuration parameters for the numerical assessment are reported in Table III. It is worthwhile noticing that we consider with $\Delta t = 16.7$ ms, computed based on OGBSC; clearly, lower values will result in a better performance, while larger values in worse result due to the reduced/increased information aging at the transmitter. However, the general trends discussed below still hold. Moreover, for the following system-level analyses, only the value of Δt impacts the results and not the specific choice of an OGBSC or OBBSC design.

A. Simulation Scenarios and Assumptions

The users are uniformly distributed in the coverage area. It shall be noticed that, considering the large on-ground coverage, the users' distribution can be nonuniform, with

TABLE III
System Configuration Parameters for the Numerical Assessment

Parameter	Value
Transmission EIRP	$0, 4, 8, 12$ dBW/MHz
Channel model	clear sky, NLOS
Propagation environment	dense urban
Carrier frequency	S-band (2 GHz)
User bandwidth	30 MHz
Receiver type	fixed VSAT/handheld (antenna parameters in TR 38.821 [66])
N_F	32×32 UPA, 0.55λ spacing
Nodes per swarm N_{node}	$1, 2$
Altitude	600 km
Beams per node $N_{B,\text{node}}$	$91(N_{\text{node}} = 1), 61(N_{\text{node}} = 2)$
User density	0.5 users/km^2
Aging interval Δt	16.7 ms
Scheduling	random

hot and cold traffic spots in densely and scarcely populated areas, respectively; however, in this work we do not focus on scheduling aspects and, thus, assuming a uniform distribution does not impact the generality of the proposed federated CF-MIMO system. Based on the user density reported in Table III, approximately 30 000 users are considered. The UEs are assumed to be fixed; in fact, by means of extensive numerical simulations, it was observed that for users moving at up to 250 km/h the performance loss was in the order of 10^{-4} b/s/Hz in terms of spectral efficiency, i.e., negligible. To provide connectivity to the uniformly distributed users, the UPA on-board each node is designed as a square lattice with $N_F = 1024$ radiating elements; the spacing between adjacent elements is fixed at 0.55λ. Notably, the radiation pattern from the nth element on the sth node in the direction of the ith user, identified by the direction cosines coordinates $\mathbf{p}_{i,s}^{(t)} = \left[u_{i,s}^{(t)}, v_{i,s}^{(t)} \right]$ at the tth time instant, is given by [64]

$$g_{i,n,s}^{(TX,t)} = g_{E,i}^{(t)} e^{jk_0 \mathbf{r}_{n,s} \cdot \mathbf{p}_{i,s}^{(t)}} \qquad (18)$$

where $g_{E,i}$ is the radiation pattern of the single radiating element in the direction of the ith user $\mathbf{r}_{n,s}$ the position of the nth element on the sth UPA. The element pattern $g_{E,i}$ is assumed to be the same for all radiating elements and computed as in Section V-A of ITU-R M.2101 [67].

We consider both centralized ($N_{\text{node}} = 1$) and federated ($N_{\text{node}} = 2$) configurations. Notably, configurations with more than two nodes might be considered; however, this would significantly increase the dimensions of the channel and beamforming matrices, as for each additional node there are KN_F additional complex coefficients. Moreover, as of today, in the framework of NTN systems all technologies considering multiple transmission points (e.g., multiconnectivity, coherent, and noncoherent joint transmission) are considering two flying nodes. In order to provide a fair comparison between CF (MMSE, LB-MMSE) and beam-based (SS-MMSE, MB) algorithms, each node in the swarm generates $N_{B,\text{node}}$ beams organized in an hexagonal lattice on-ground. The number of beams per node is different in the two scenarios so as to obtain a similar number of beams
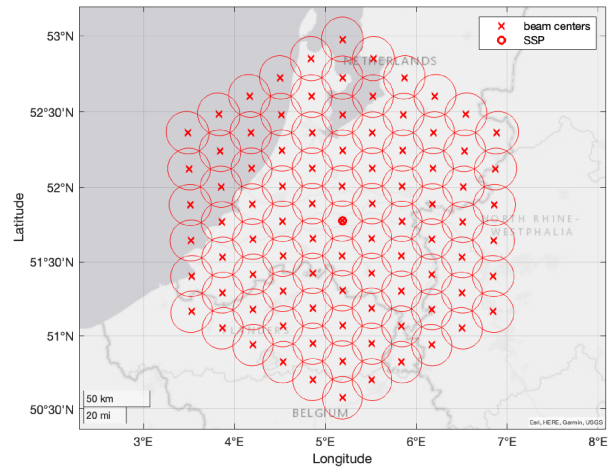

Fig. 4. Centralized ($N_{\text{node}} = 1$) scenario. Coverage centered around the subsatellite point.

per swarm N_B (91 with $N_{\text{node}} = 1$ and 122 with $N_{\text{node}} = 2$). Moreover, it shall be noticed that, with multiple nodes, each node in the swarm generates its corresponding lattice, but then it covers all of the beams created by the swarm. Figs. 4 and 5 show the on-ground beam footprints with $N_{\text{node}} = 1$ and $N_{\text{node}} = 2$, respectively. With multiple nodes, the fact that each node is initially generating a single beam lattice leads to beams that significantly overlap at the border between the two lattices, i.e., there are beams that have their centers inside other beams boundaries at less than -3 dB. Notably, when implementing MIMO techniques, this might lead to a performance loss [34], [47]; in particular, two UEs selected from two of such beams might be scheduled in the same time slot. In this case, the two users have very similar channel signatures (CSI coefficients) and, thus, the channel matrix to be inverted in MMSE-like solutions might be ill-conditioned. To circumvent this issue, proper scheduling algorithms might be implemented; in the following, we assume that the RRM algorithm avoids such situations by activating only one beam among those in which the relative distance among the beam centers does not guarantee a 3-dB
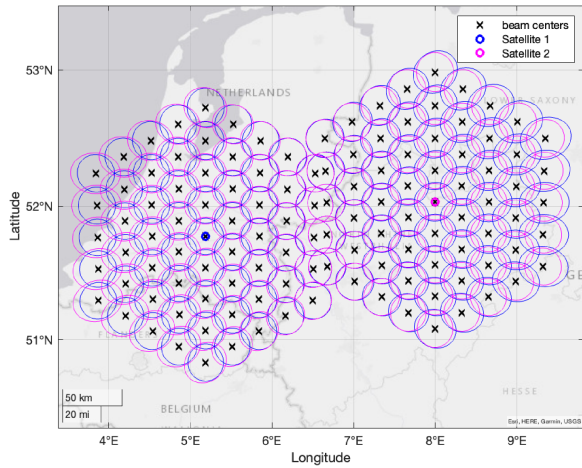
Fig. 5. Federated ($N_{\mathrm{node}} = 2$) scenario. Blue lines represent the footprint of satellite 1 and magenta lines those for satellite 2.
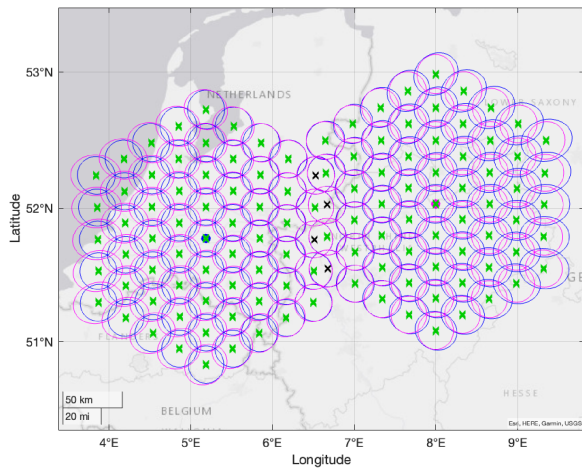

Fig. 6. Example of RRM algorithm activating a subset of beams (green) to avoid an ill-conditioned channel matrix due to beam proximity issues.

separation. An example is shown in Fig. 6. Consequently, to provide a fair comparison between the centralized and federated scenarios, the available power per node is scaled to guarantee that the same average power per beam is available

$$P_{t,\mathrm{node}} = P_t \frac{N_{B,\mathrm{multi}}}{N_{\mathrm{node}} N_{B,\mathrm{single}}} \tag{19}$$

where $P_{t,\mathrm{node}}$ is the available power per node, and $N_{B,\mathrm{single}}$ and $N_{B,\mathrm{multi}}$ are the number of active beams with $N_{\mathrm{node}} = 1$ and $N_{\mathrm{node}} = 2$, respectively. It can be noticed that when all beams are active in the multiple nodes case (i.e., there is no beam proximity issue): 1) if $N_{B,\mathrm{multi}} = N_{\mathrm{node}} N_{B,\mathrm{single}}$, i.e., each node in the swarm generates the same amount of beams as in the centralized case, then $P_{t,\mathrm{node}} = P_t$ and 2) if $N_{B,\mathrm{multi}} = N_{B,\mathrm{single}}$, i.e., the same number of beams is generated independently of the number of nodes, $P_{t,\mathrm{node}} = P_t / N_{\mathrm{node}}$. Referring to Figs. 5 and 6, there are 118 active beams compared with 91 with a single node; a transmission power density of 4 dBW/MHz leads to

$P_t = 18.77$ dBW over a 30-MHz bandwidth and to $P_{t,\mathrm{node}} = 16.89$ dBW/MHz.

With respect to scheduling, a random algorithm is implemented [34], [37]: in each time slot, one UE per beam is randomly selected and the total number of time slots is computed so as to guarantee that all UEs are served at least once. The coverage is based on Earth-moving beams, i.e., the beams move together with the NGSO nodes along their orbits. It is worthwhile highlighting that a beam lattice is only needed for the MB and SS-MMSE solutions; MMSE and LB-MMSE allow to implement CF-MIMO, as long as an advanced scheduler operating exclusively on the location or CSI vectors is implemented. Thus, the concept of beams for MMSE and LB-MMSE is only exploited for the random scheduler and to have a comparison with MB and SS-MMSE. Two channels are considered: 1) clear sky, in which no additional loss is present, i.e., $L_{i,s}^{(t)} = 1 \ \forall i, s, t$ and 2) NLOS, modeled as described in Section III-E assuming a dense-urban environment, i.e., the worst conditions in terms of CL and σ_{SHA}. In the latter scenario, a UE is in LOS or NLOS conditions according to the probabilities reported in TR 38.821 [62] as a function of its elevation angle.

B. Key Performance Indicators

Below, we discuss the numerical results obtained with both ideal and nonideal information to compute the beamforming matrix. The performance is provided in terms of average spectral efficiency in [b/s/Hz] and percentage of unserved users. To this aim, it shall be mentioned that, based on the truncated Shannon bound in (8), the average spectral efficiency is computed only on the UEs, which are served by the system, i.e., those for which the SINR is above γ_{min}. The percentage of unserved users is computed as the percentage of users with SINR below γ_{min}.

For the sake of completeness, it is worthwhile highlighting that NTN systems currently assume frequency division duplexing (FDD) operation, due to the large propagation delays that make time DD (TDD) approaches significantly less efficient. In the considered S-band, two allocations are possible [68]: band n256 (1980–2010 MHz on the UL and 2170–2200 MHz on the DL) and n255 (1626.5–1660.5 on the UL and 1525–1559 MHz on the DL). The CSI is estimated through the CSI-RS on the DL and then reported to the network element computing the beamforming matrix, for CSI-based solutions. With location-based approaches, this is not impacting the architecture or required signaling, as the UEs estimate their positions and then the network estimates the channel coefficients. In S-band, 3GPP Rel. 17 foresees the deployment of handheld terminals. However, in this article, we also consider VSAT users in order to assess the impact of a omnidirectional receiving antenna (handheld) compared with directive radiation patterns (VSAT). In this context, it shall be mentioned that the target performance for handheld terminals in 5G and 5G-A is in the order of a few Mbps; however, it is expected that in 6G NTN systems the requirements will be as large as a few tens of
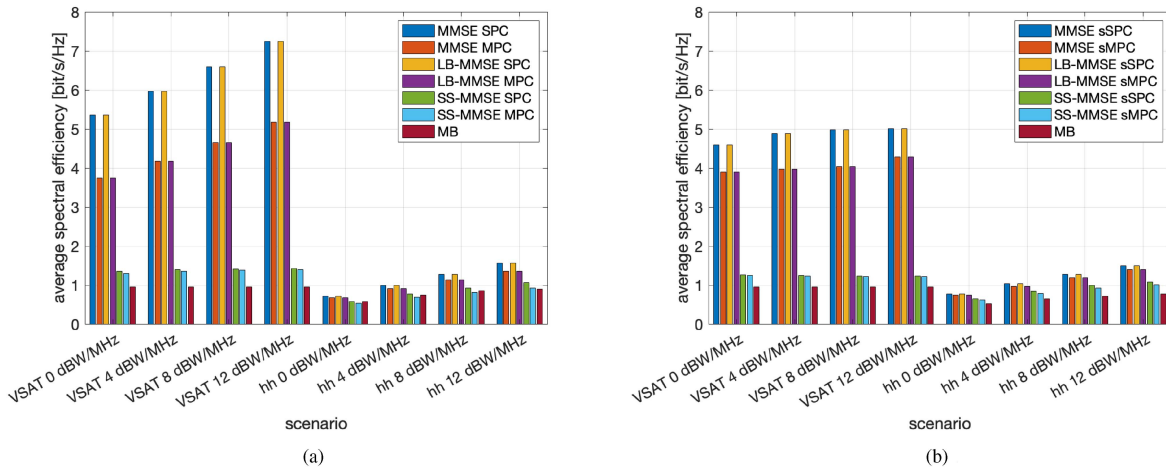
Fig. 7. Average spectral efficiency in clear sky with (a) $N_{\mathrm{node}} = 1$ and (b) $N_{\mathrm{node}} = 2$.

Mbps [5], [7], [69], thus requiring advanced solutions as those discussed in this work.

C. Ideal Information

In this section, we discuss the numerical results under ideal conditions, i.e., ideal CSI estimation (MMSE), ideal location estimation (LB-MMSE, SS-MMSE, MB), and ideal knowledge of the radiation pattern (LB-MMSE and SS-MMSE). It is worthwhile mentioning that, despite the ideal conditions, there is still a misalignment between the beamforming matrix $\mathbf{W}^{(t_0)}$ and the channel matrix $\mathbf{H}^{(t_1)}$ because of the movement of the swarm nodes on their orbits.

Clear-sky conditions:

Fig. 7 shows the average spectral efficiency in clear-sky conditions with $N_{\mathrm{node}} = 1$ (standalone) and $N_{\mathrm{node}} = 2$ (federated). The following general trends can be observed.

1) MMSE and LB-MMSE provide the best performance for all transmission power densities and terminal types. Moreover, they provide the same performance; this is motivated by observing that, in the absence of additional losses and with ideal estimations, the channel coefficients in (3) and (10) are identical. The performance of the SS-MMSE and MB solutions are significantly worse, with losses in the order of 6 and 4 b/s/Hz with VSATs in the centralized and federated scenarios.
2) As expected, the (s)SPC normalization provides the best performance. However, this solution provides a theoretical upper bound but it is not feasible. With (s)MPC, the performance is worse in particular in systems with large received power (VSAT and large power density); this is motivated by the fact that the (s)MPC normalization does not exploit the entire available power.
3) Handheld terminals have a worse performance compared with VSATs, due to the omnidirectional antennas. The different techniques and normalizations provide a similar performance with low EIRP (in

this case, the performance is more noise limited than interference limited), while with larger transmission power levels interference increases and the impact of a different technique or normalization becomes slightly more evident.

Comparing the performance between the centralized and federated scenarios, interestingly, the following can be noticed.

1) With both handheld and VSAT terminals, the spectral efficiency is larger for increasing values of the power density. However, with multiple nodes and VSATs, the performance tends to saturate with large power levels. Fig. 8 shows the cumulative distribution function (CDF) of the SNR and SIR with MMSE beamforming. It can be observed that, clearly, the SNR is always improved by increasing the power density; however, the SIR is slightly worse with larger power with $N_{\mathrm{node}} = 2$, while with $N_{\mathrm{node}} = 1$ it is improved. Thus, with multiple nodes in the swarm interference cancellation is critical. This is motivated by observing that, with N_{node} nodes there are $N_{\mathrm{nodes}}N_F$ radiating elements; this leads to an increased sensitivity to any misalignment between $\mathbf{W}^{(t_0)}$ and $\mathbf{H}^{(t_1)}$. Moreover, also the block sSPC and sMPC normalizations with multiple nodes increase such misalignment.
2) The performance with VSATs and $N_{\mathrm{node}} = 2$ is beneficial only at low power and with (s)MPC. In all other cases, i.e., when the interference to be dealt with by the beamformer is increased, the centralized scenario provides a better result.
3) With handheld terminals, the average spectral efficiency is typically slightly better (0.05–0.1 b/s/Hz) with $N_{\mathrm{node}} = 2$. The only exception is when the power density is large and (s)SPC normalizations are considered. However, in this case, we should also observe the percentage of unserved users, reported in Fig. 9. In the centralized case, there are no
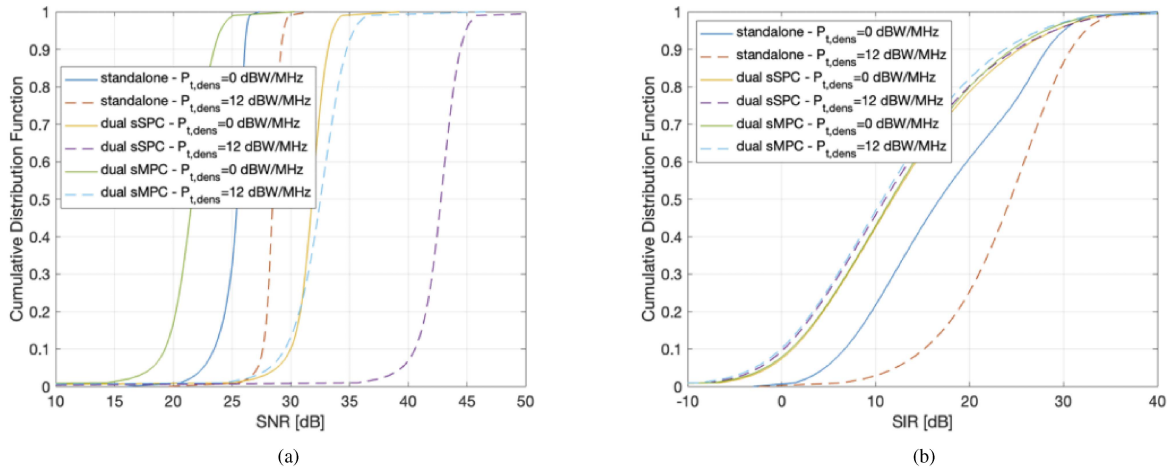
Fig. 8. CDF of the (a) SNR and (b) SIR with MMSE beamforming and VSATs. For the centralized case, SPC is considered.
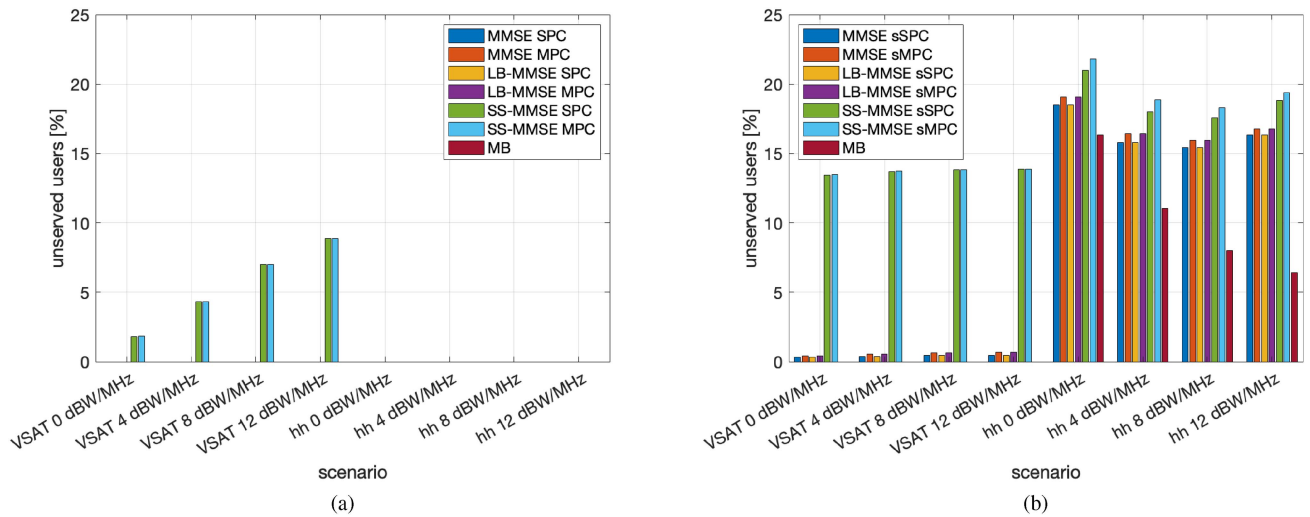

Fig. 9. Percentage of unserved users in clear sky with (a) $N_{\text{node}} = 1$ and (b) $N_{\text{node}} = 2$.

users in outage with MMSE and LB-MMSE; with SS-MMSE, based on an approximation of the UEs' locations, the impact of a larger transmission power is more detrimental for the interference cancellation capability and the outage increases. With two nodes, the situation is worse. In particular, the following holds.

a) With SS-MMSE, there are many unserved users with both terminal types (up to 22%). This is motivated by the much larger number of radiating elements and the consequent impact on any misalignment between $\mathbf{W}^{(t_0)}$ and $\mathbf{H}^{(t_1)}$, more evident in this case due to the further approximation in the UEs' locations.

b) There is a slight outage also with MMSE/LB-MMSE and VSATs, always below 0.7%, motivated as above. With VSATs, the impact of such misalignment is limited by the presence of directive antennas.

c) With MMSE/LB-MMSE and handheld terminals, the outage is significantly higher (up to 19% in some cases) and it tends to decrease

for increasing power levels. This trend is motivated by the omnidirectional antennas at the receiver. In fact, VSATs are assumed to be ideally pointing and tracking the node providing the best radiation pattern, thus limiting the residual intraswarm interference. Handheld terminals do not have directive radiation patterns and, thus, they are significantly more subject to the residual intraswarm interference. This behavior is shown in Fig. 10.

NLOS dense-urban conditions:

Figs. 11 and 12 show the performance on the NLOS dense-urban channel. In general, we can observe that the performance is worse compared with clear-sky conditions in all cases, as expected. Moreover, the following holds.

1) The LB-MMSE algorithm has a slightly worse performance compared with MMSE. Since this channel includes the additional losses, which are not taken into account by LB-MMSE, the misalignment between $\mathbf{W}^{(t_0)}$ and $\mathbf{H}^{(t_1)}$ is larger with this algorithm. However, considering all of the advantages that
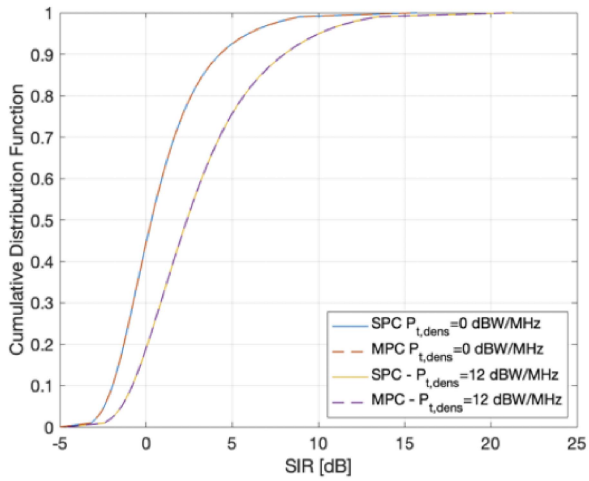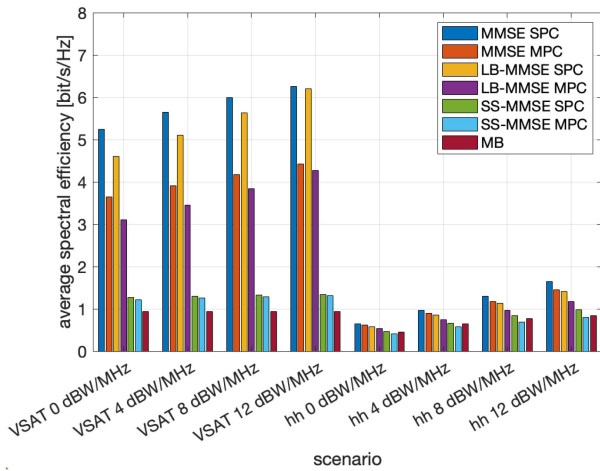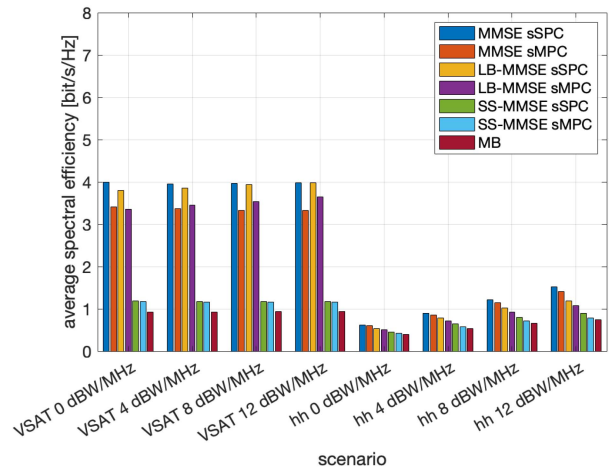
(a)
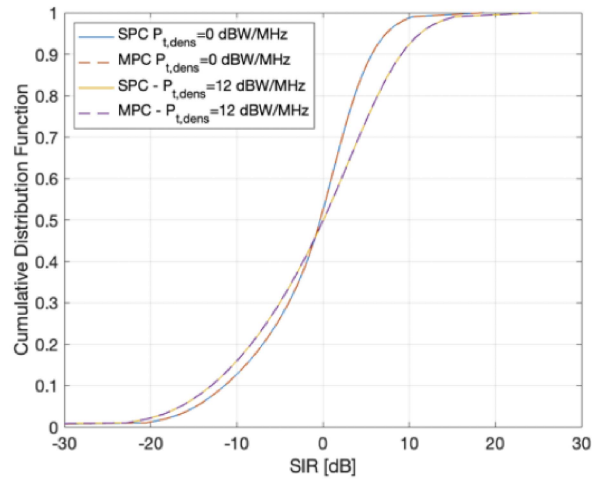
(b)

Fig. 10. CDF of the SIR in the (a) centralized—$N_{node} = 1$ and (b) federated—$N_{node} = 2$ scenarios with MMSE beamforming and handheld terminals.
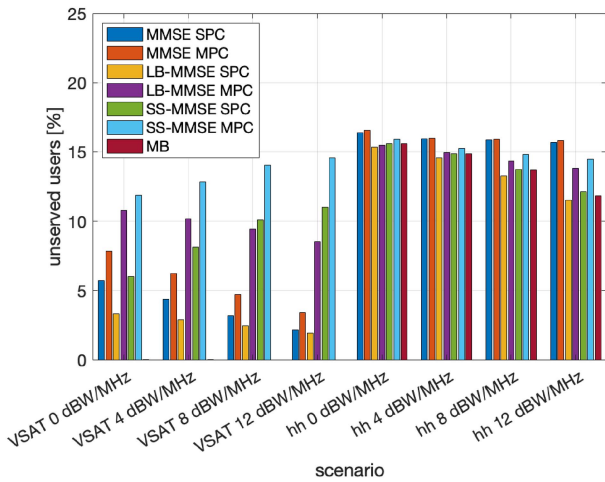

(a)
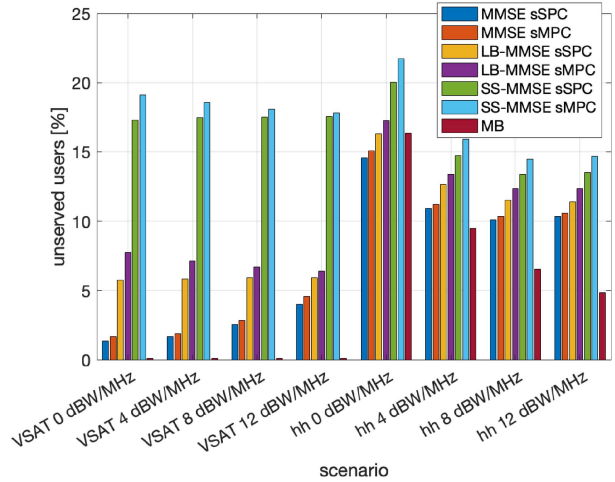

(b)

Fig. 11. Average spectral efficiency in NLOS dense-urban conditions with (a) $N_{node} = 1$ and (b) $N_{node} = 2$.

(a)

(b)

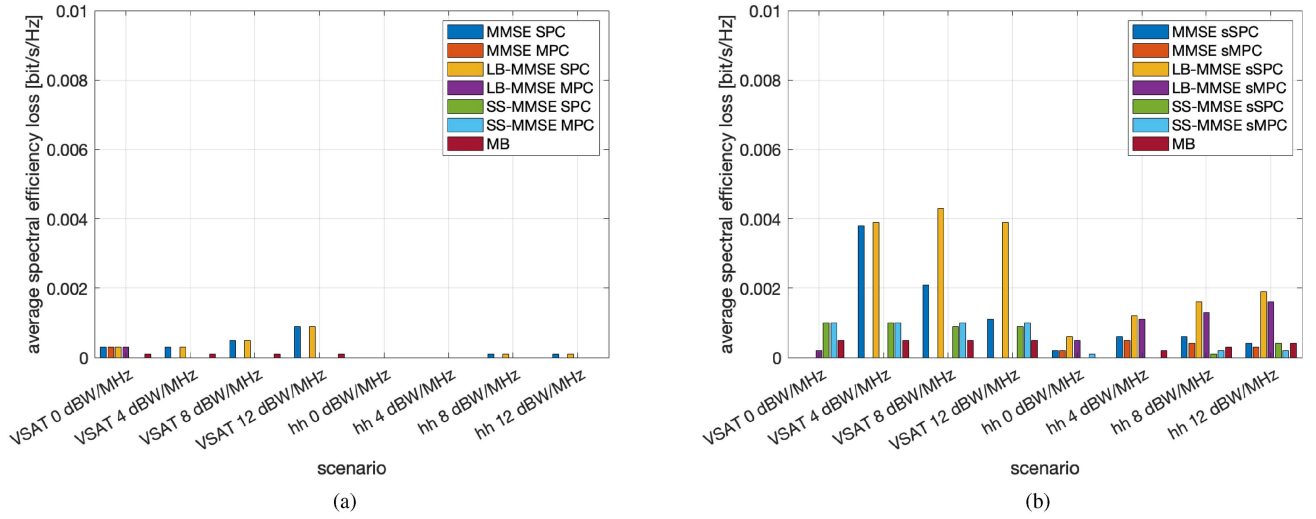Fig. 12. Percentage of unserved users in NLOS dense-urban conditions with (a) $N_{node} = 1$ and (b) $N_{node} = 2$.

Fig. 13. Loss in the average spectral efficiency in clear-sky conditions with (a) $N_{\text{node}} = 1$ and (b) $N_{\text{node}} = 2$.

location-based solutions provide, extensively discussed in Section III-D, this algorithm is indeed a viable and effective approach to implement CF-MIMO in NTN systems. The performance with SS-MMSE and MB is still much worse compared with MMSE and LB-MMSE, with a loss in the spectral efficiency up to 4 b/s/Hz with VSAT receivers.

2) With respect to the normalizations, as in clear-sky conditions, (s)SPC performs better than (s)MPC, which, however, is the practically implementable solution.

3) Comparing the centralized and federated scenarios, we can observe that the spectral efficiency is always better with a single node. In particular, with large transmission power and VSAT receivers, its gain can be as large as 2 b/s/Hz. However, observing the percentage of unserved users, it can be noticed that, with MMSE and LB-MMSE, the exploitation of a second node in the swarm is significantly beneficial with: 1) low transmission power and VSAT and 2) large transmission power and handheld. Thus, the exploitation of additional nodes is beneficial in harsh propagation conditions, since it introduces a gain in terms of path diversity. In dense-urban environments, the advantage of a second node in terms of outage can be: 1) with low transmission power, as large as 6.1% for MMSE-MPC with VSAT terminals and 2) with large transmission power, as large as 5.7% for MMSE-SPC with handheld terminals. In these conditions, despite the lower spectral efficiency, the system would be able to serve many more users with two nodes.

D. Nonideal Information

In this section, we discuss the performance obtained when nonideal information on the UEs' position and the radiation pattern model is considered for LB-MMSE and SS-MMSE.

a) Positioning: In this case, we assume that each user estimates its position with a uniformly distributed error of $\mathcal{U}[0, 10]$ m, in a random direction $\mathcal{U}[0, 2\pi)$, with respect to its correct location. It shall be noticed that the maximum location error is significantly larger compared with the accuracy that current receivers equipped with GNSS can achieve. This is aimed at showing the significant robustness of the proposed LB-MMSE algorithm to a nonideal estimation of the location.

Figs. 13 and 14 show the loss in the average spectral efficiency in clear-sky and NLOS dense-urban conditions, respectively. At most, the performance is degraded by 0.04 b/s/Hz. This is in line with the previous statement related to the movement of the users (i.e., even when moving at 250 km/h, the performance loss is in the order of 10^{-4} b/s/Hz). In terms of the percentage of unserved users, the loss was observed to be negligible. Thus, LB-MMSE and SS-MMSE are significantly robust to positioning errors.

b) Radiation pattern model: When computing the LB-MMSE and SS-MMSE channel coefficients based on the UEs' location, another source of error is the nonideal representativeness of the radiation pattern model. To model this impairment, we focus on the on-board radiation pattern model. In particular, we assume that the estimated antenna radiation between the nth element on-board the sth satellite and the kth user at the tth time instant, $\widehat{g}_{k,n,s}^{(TX,t)}$, is given by

$$\widehat{g}_{k,n,s}^{(TX,t)} = g_{k,n,s}^{(TX,t)} + \Delta g_{k,n,s}^{(TX,t)} \tag{20}$$

where $\Delta g_{k,n,s}^{(TX,t)} = \left| \Delta g_{k,n,s}^{(TX,t)} \right| e^{-j\angle \Delta g_{k,n,s}^{(TX,t)}}$ is an r.v. modeling the error on the radiation pattern with the following amplitude and phase statistics:

$$\left| \Delta g_{k,n,s}^{(TX,t)} \right| \sim \mathcal{N}\left(0, \left| g_{k,n,s}^{(TX,t)} \right|^2 \varepsilon_{rp} \right) \tag{21}$$
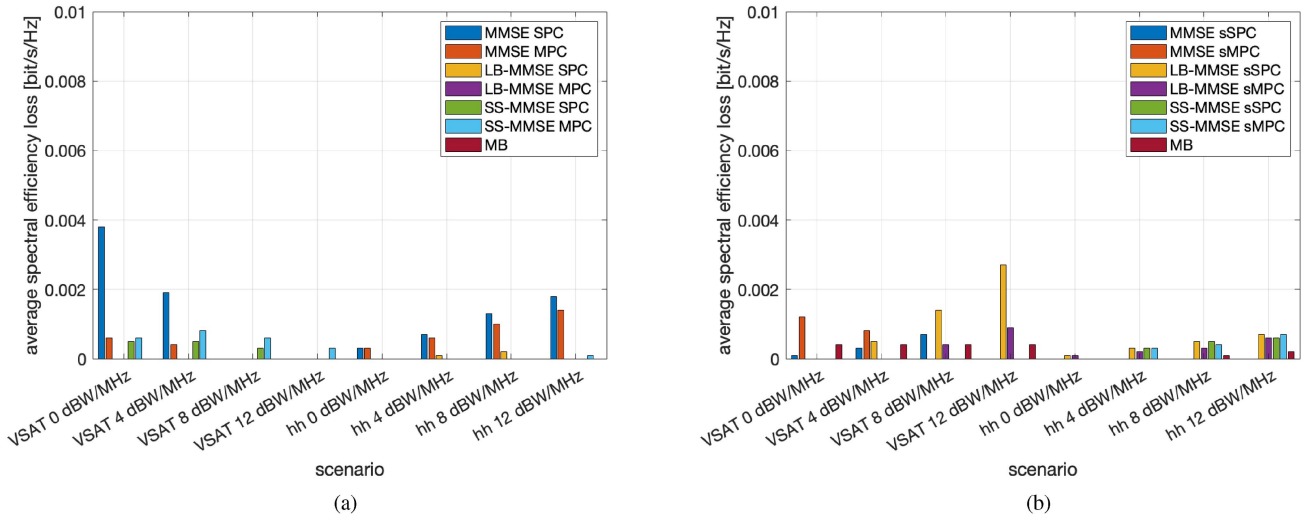
Fig. 14. Loss in the average spectral efficiency in NLOS dense-urban conditions with (a) $N_{\text{node}} = 1$ and (b) $N_{\text{node}} = 2$.
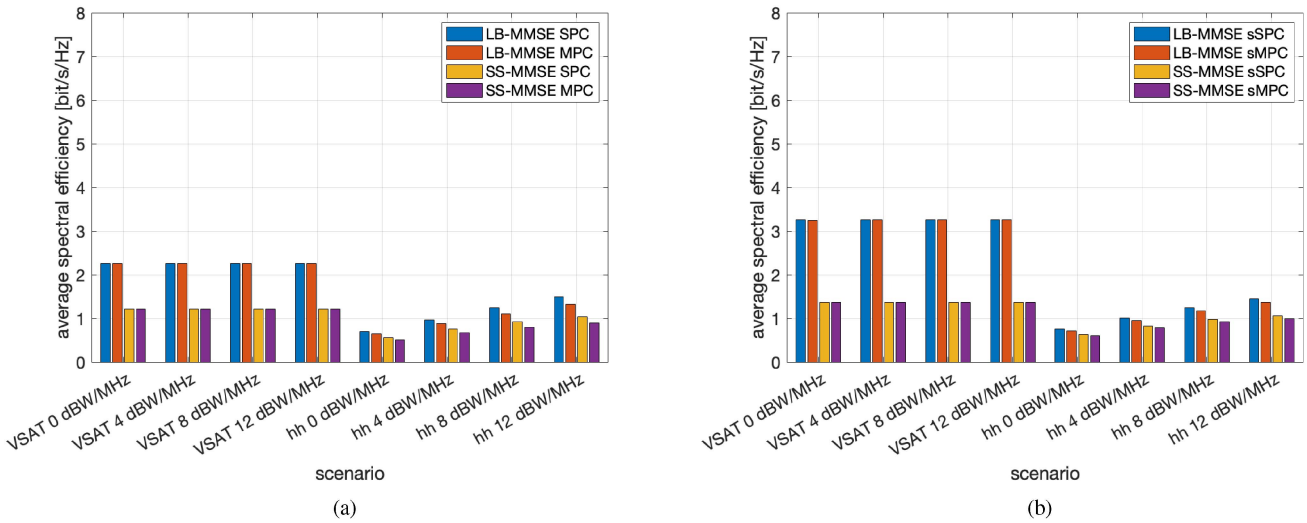

Fig. 15. Average spectral efficiency in clear sky with (a) $N_{\text{node}} = 1$ and (b) $N_{\text{node}} = 2$ and nonideal radiation pattern.

$$\angle \Delta g_{k,n,s}^{(TX,t)} \sim \mathcal{N}\left(0, \left|\angle g_{k,n,s}^{(TX,t)}\right|^2 \varepsilon_{rp}\right). \qquad (22)$$

The coefficient ε_{rp} allows to adjust the variance of the amplitude and phase errors.[7] In the following, we assume $\varepsilon_{rp} = 0.05$, i.e., a 5% error on the correct amplitude and phase of the radiation pattern.

Figs. 15 and 16 show the average spectral efficiency for the LB-MMSE and SS-MMSE algorithms and $\varepsilon_{rp} = 0.05$. It can be noticed that both algorithms are particularly impacted by a nonideal knowledge. The loss with VSATs

in the centralized scenario can be as large as 4.5 b/s/Hz and 3.5 b/s/Hz in clear-sky and NLOS dense-urban conditions, respectively; with federated solutions and two nodes, the performance is less degraded, since the system benefits from the transmission from distributed sources, and the loss is in the order of 1–1.5 b/s/Hz. With handheld terminals, the performance with two nodes is still better, but the advantage is more limited compared with the centralized case.

In terms of unserved users, some interesting behaviors arise. In particular, with VSAT terminals the performance with an error on the radiation pattern model is actually improved in terms of outage, while this phenomenon is absent for handheld terminals. Figs. 17 and 18 show the outage reduction representing such gain; it can be noticed that in the centralized scenario this phenomenon is more relevant. To understand the motivation for this behavior, let us focus on the centralized case in NLOS dense-urban conditions, where it is more evident. In particular, Figs. 19

---

[7]It shall be noticed that information on such errors is not available and it is impacted by many factors, including the UPA manufacturing, materials, possible damages during the satellite launch and orbital manoeuvers, etc. The same error is adopted for both the amplitude and phase of the coefficients as modifying the real and imaginary parts would mix these contributions and be less intuitive.
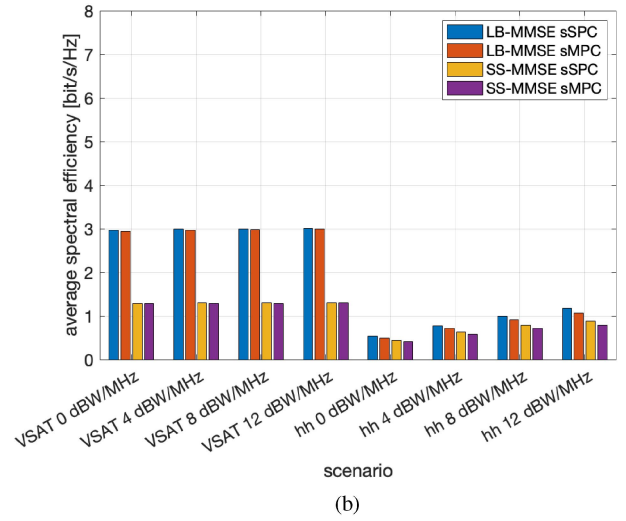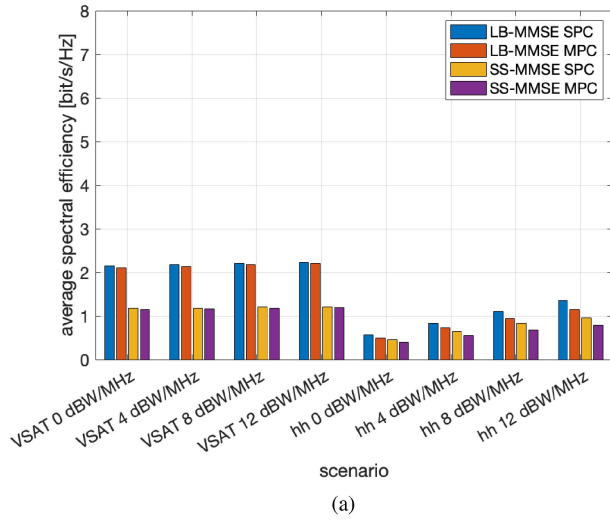
Fig. 16. Average spectral efficiency in NLOS dense-urban conditions with (a) $N_{\text{node}} = 1$ and (b) $N_{\text{node}} = 2$ and nonideal radiation pattern.
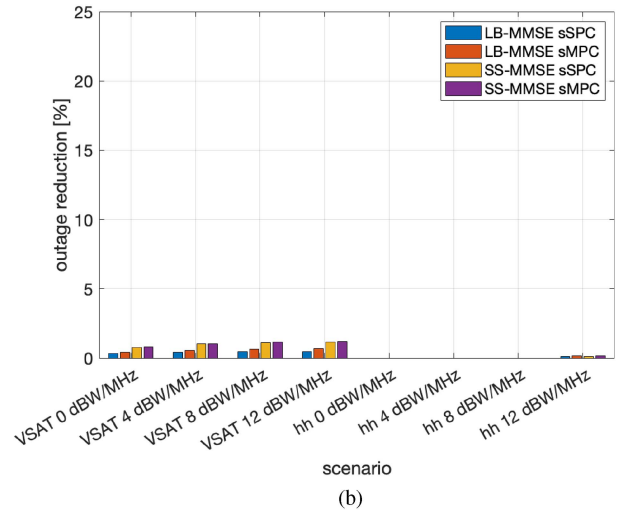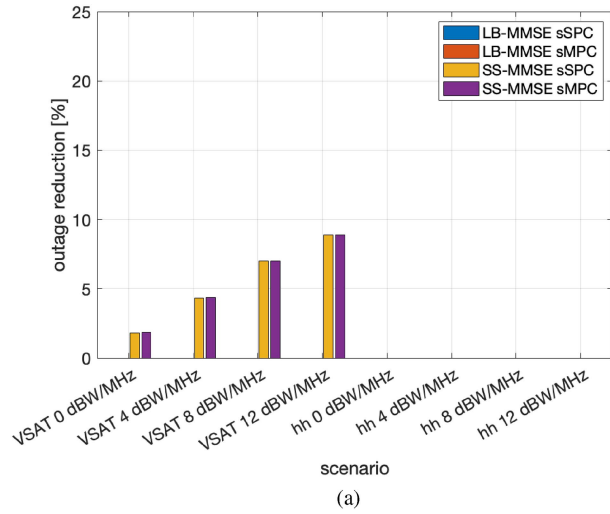

Fig. 17. Reduction in the percentage of unserved users in clear sky with (a) $N_{\text{node}} = 1$ and (b) $N_{\text{node}} = 2$ and $\varepsilon_{rp} = 0.05$.
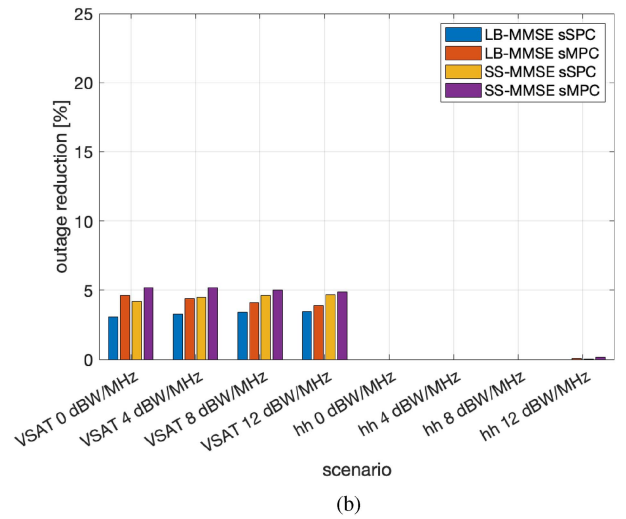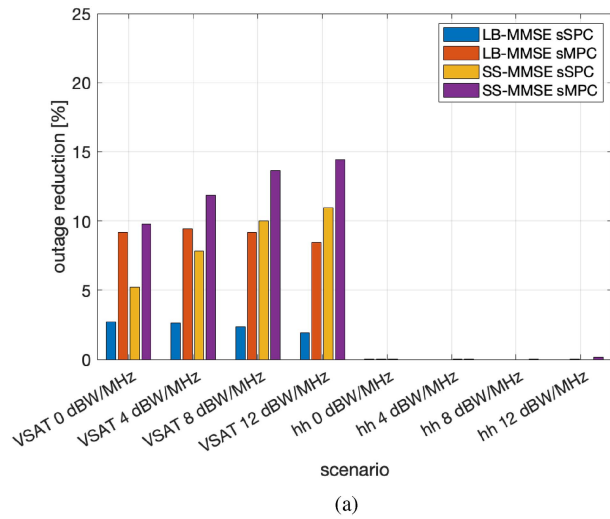

Fig. 18. Reduction in the percentage of unserved users in NLOS dense-urban conditions with (a) $N_{\text{node}} = 1$ and (b) $N_{\text{node}} = 2$ and $\varepsilon_{rp} = 0.05$.

Fig. 19. Geographical distribution of the SINR over ten time slots with (a) LB-MMSE and (b) SS-MMSE in NLOS dense-urban conditions with $\varepsilon_{rp} = 0$ and a centralized node.
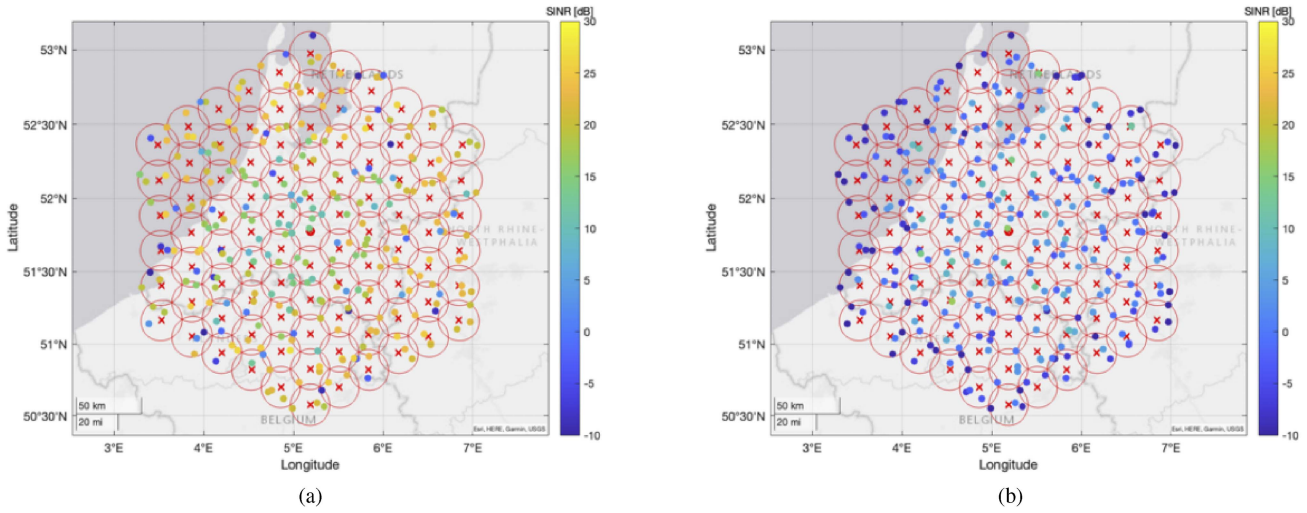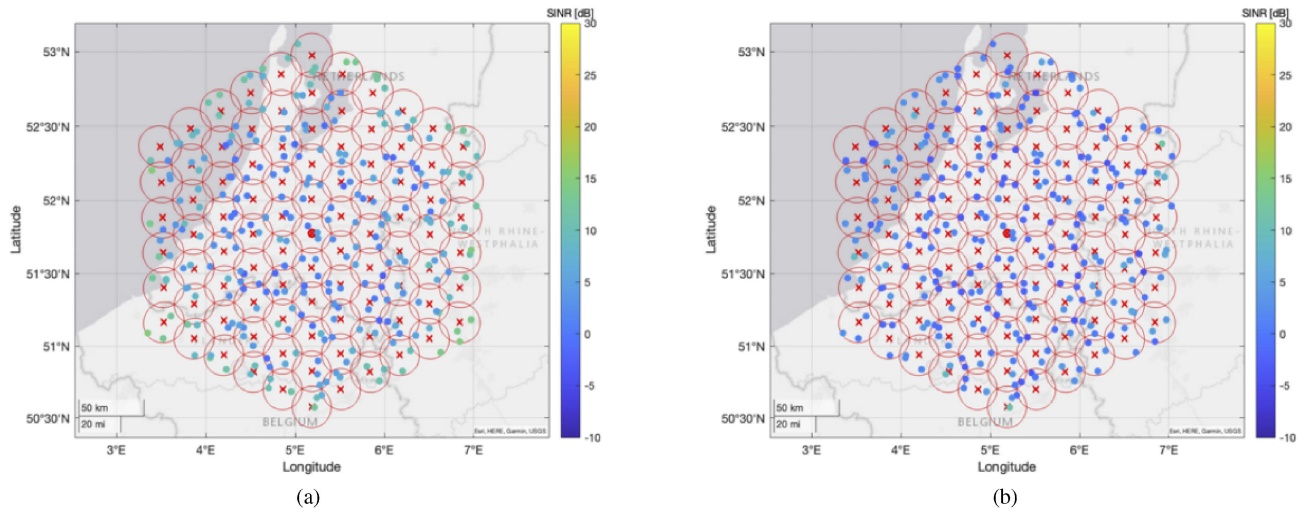

Fig. 20. Geographical distribution of the SINR over ten time slots with (a) LB-MMSE and (b) SS-MMSE in NLOS dense-urban conditions with $\varepsilon_{rp} = 0.05$ and a centralized node.

and 20 show the geographical distribution of the SINR with $\varepsilon_{rp} = 0$ (ideal), and $\varepsilon_{rp} = 0.05$, respectively. The following can be noticed.

1) With LB-MMSE and $\varepsilon_{rp} = 0$, the users in the outer part of the coverage are those in the best channel conditions; the uniformly distributed users that are experiencing a bad SINR are those in NLOS conditions, which include the CL and a harsh standard deviation of the shadow fading. The best behavior at the coverage edge is due to the combination of the reduced interference in the external areas of the coverage region and the nature of LB-MMSE, which is a user-centric technique in which the CSI vectors are identified specifically per user without approximations, compared with SS-MMSE. When $\varepsilon_{rp} = 0.05$, the performance at the edge of the coverage is still better compared with the inner area, but in general the SINR is significantly lower and

much more uniformly distributed, leading to a loss in the spectral efficiency and a gain in the outage, since all users are now above the SINR threshold. The error on the radiation pattern is making the CSI vectors more uniform from the beamformer perspective and all users are served with a similar SINR (as also demonstrated by the constant performance in Figs. 17 and 18 for increasing values of the power density). This is further substantiated in Fig. 21, which shows the power allocated to the users in a time slot with LB-MMSE: 1) in ideal conditions, the users at the coverage edge are allocated less power because they experience less interference and have large antenna gains and 2) when errors are introduced, power tends to be uniformly distributed across the beams, since the users' CSI vectors tend to be more and more similar.

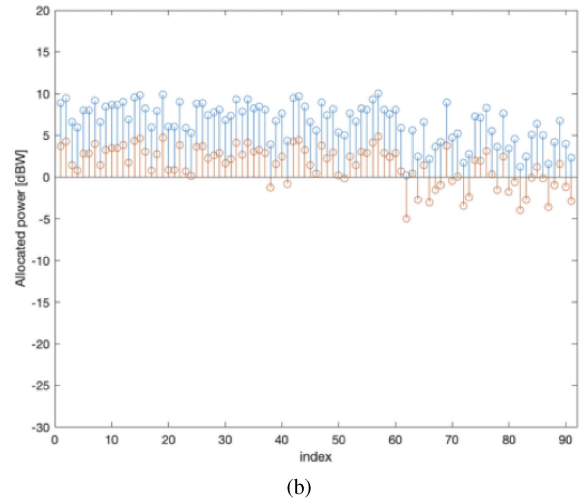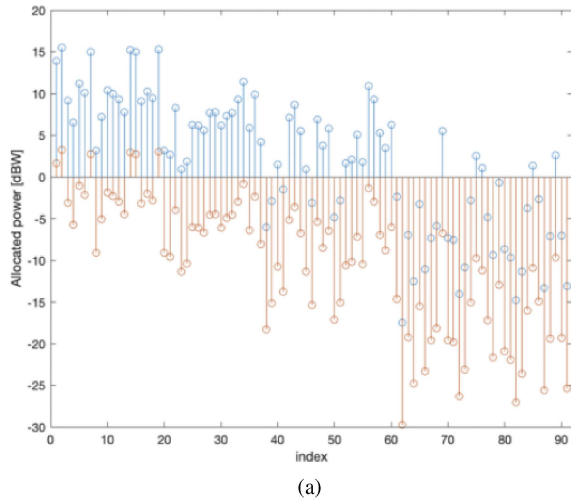2) SS-MMSE is a beam-based algorithm, as each user is approximated with the closest beam center. Thus,

Fig. 21. Power allocation per served user with LB-MMSE with centralized MIMO. (a) $\varepsilon_{rp} = 0$. (b) $\varepsilon_{rp} = 0.05$.
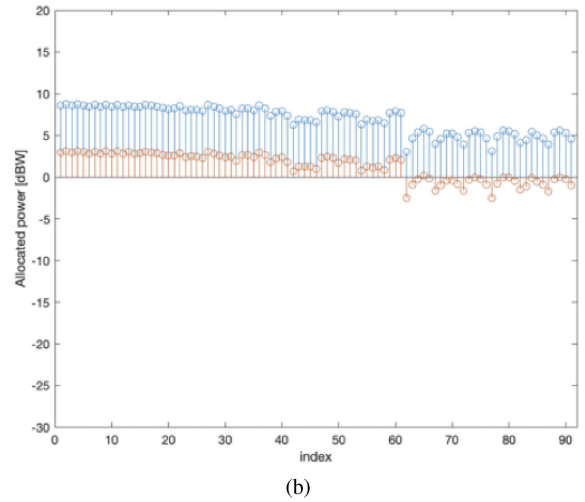

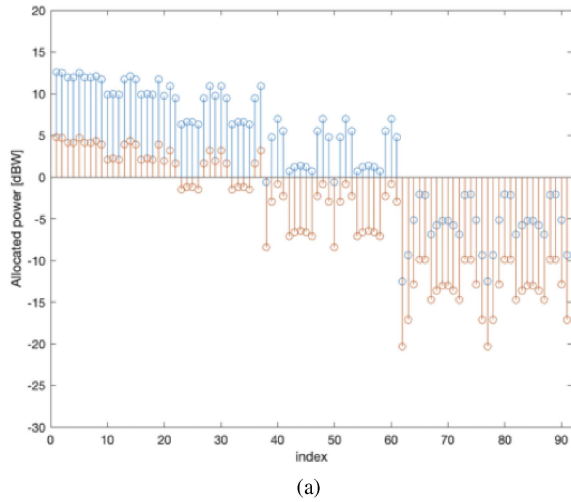Fig. 22. Power allocation per served user (beam) with SS-MMSE with centralized MIMO. (a) $\varepsilon_{rp} = 0$. (b) $\varepsilon_{rp} = 0.05$.

the performance is driven by the distance from the associated beam center: the larger this distance, the larger the approximation and, consequently, the worst the performance. In addition to this aspect, also with SS-MMSE the external beams are allocated a lower power; however, differently from LB-MMSE, the reduced interference in the external tiers is not sufficient to cope with both the lower allocated power and the approximation in the channel coefficients. Thus, the external tiers experience a worse performance compared with the inner ones. When $\varepsilon_{rp} = 0.05$, the same phenomenon described above for LB-MMSE arises. The CSI vectors tend to become more similar from the beamformer perspective and a uniform performance is achieved across the coverage area. This is substantiated in Fig. 22, with a very limited variability in the power allocations to the beams when $\varepsilon_{rp} = 0.05$. As observed above, the consequence is that the spectral efficiency is worse compared with the ideal scenario, while the outage is improved since users at the coverage edge that were

below the SINR threshold now experience an SINR close to that of all users.

The above phenomenon is still present for SS-MMSE in clear sky, while for the LB-MMSE it is not. In clear-sky conditions, no user is experiencing the shadow fading or CL; thus, with an algorithm in which the actual locations are used (and not an approximation), no user is in outage at the coverage edge and only the loss in the spectral efficiency is present. Similar considerations and observations can be made for the federated scenario.

E. Frequency Reuse

To conclude the extensive numerical assessment of the considered CF-MIMO techniques, we now discuss the comparison with legacy frequency reuse schemes with three and four colors (FR3 and FR4) implemented with a single node. To this aim, we consider the (s)MPC normalization only. Figs. 23 and 24 show the average capacity in clear-sky and NLOS dense-urban conditions, respectively. It can be noticed that the advantage of using an FFR scheme is
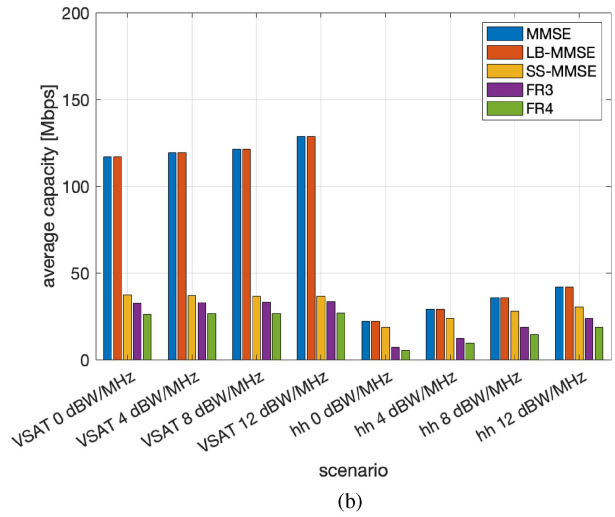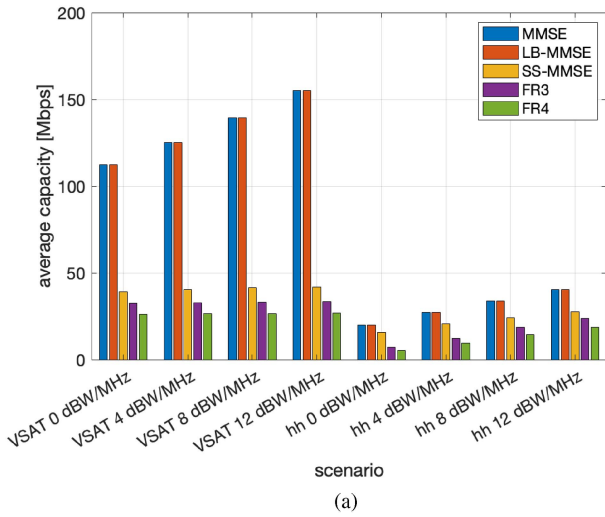
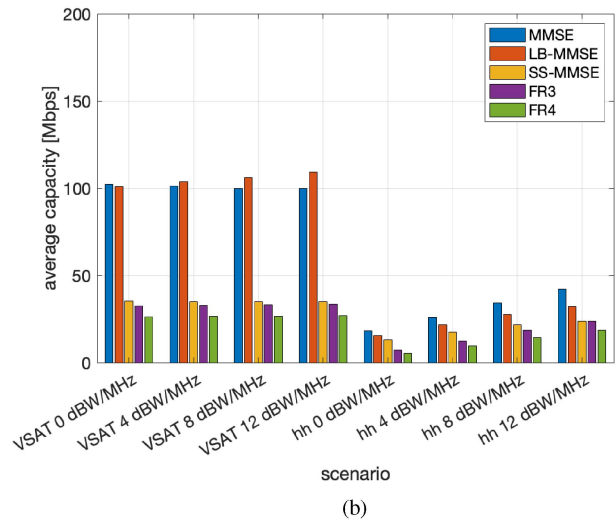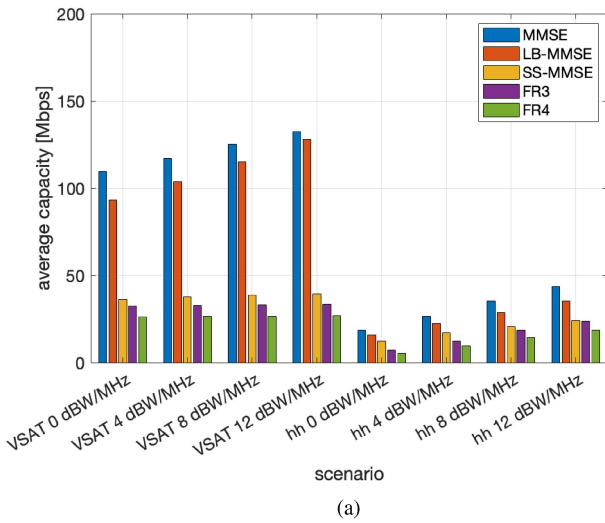Fig. 23. Average capacity in clear sky with (a) $N_{node} = 1$ and (b) $N_{node} = 2$.

Fig. 24. Average capacity in NLOS dense-urban conditions with (a) $N_{node} = 1$ and (b) $N_{node} = 2$.

significant: 1) for VSAT receivers, the gain is in the order of 100 Mbps in NLOS dense-urban conditions and even larger in clear sky and 2) with handheld terminals, the gain is in the order of 15–20 and 20–35 Mbps for clear-sky and NLOS dense-urban environments, respectively. In terms of outage, the following holds.

1) It was observed that no unserved users are present with three and four colors in clear-sky conditions; the outage performance of CF-MIMO on this channel (see Fig. 9) showed that for the (s)MPC normalization a significant amount of unserved users was present only with two nodes and handheld terminals. Thus, for VSATs and handheld terminals in the centralized scenario the advantage of FFR with CF-MIMO techniques is significant.
2) Fig. 25 shows the unserved users in NLOS dense-urban conditions. As for VSATs, it can be observed that: 1) with large transmission power, the MMSE algorithm shows a limited outage and, thus, the

advantage of CF-MIMO is clear and 2) with low transmission power, the outage is a bit larger, but it might still be acceptable considering the gain in terms of capacity. As for handheld terminals, there is a significant amount of unserved users also with FR3 and FR4. 1) In the centralized scenario, the outage is slightly below that with all CF-MIMO solutions, but considering the advantage in terms of capacity, the latter shall be selected. 2) In the federated scenario, the path diversity introduced by the additional nodes provides an advantage over FR3 and FR4 also in terms of outage.

In conclusion, the capacity is significantly improved with CF-MIMO and FFR. However, by also taking into account the percentage of unserved users, there are some scenarios in which legacy systems might still be better, e.g., with VSAT terminals and low transmission power. In all other cases, the CF-MIMO approach is by far the best system-level solution.
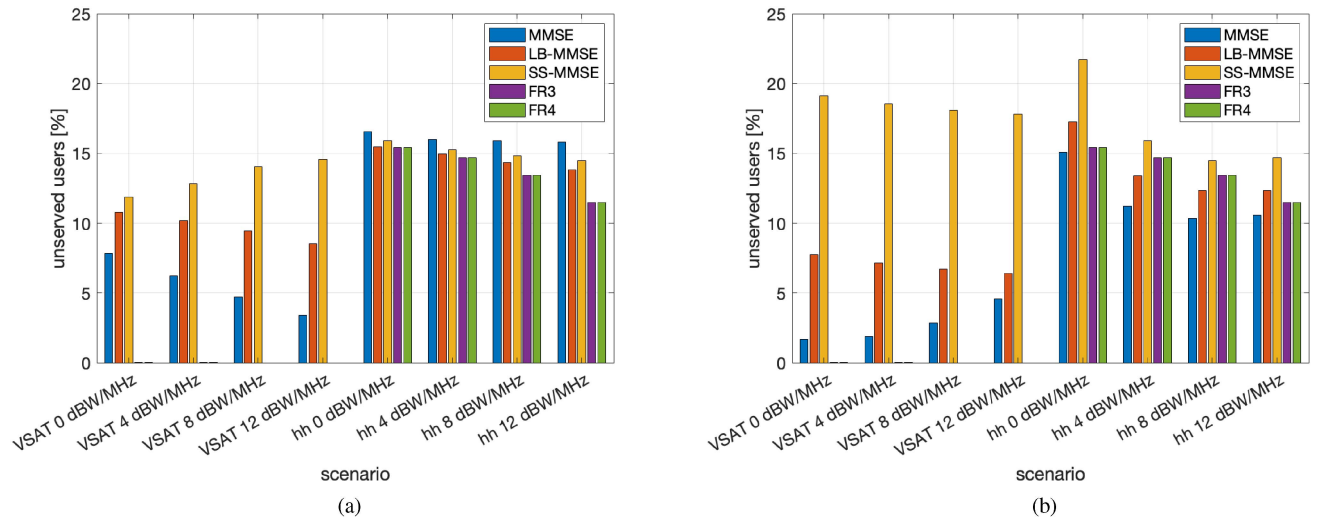
Fig. 25. Percentage of unserved users in NLOS dense-urban conditions with (a) $N_{node} = 1$ and (b) $N_{node} = 2$.

F. Recommendations

Focusing on the (s)MPC normalization, which is the feasible solution avoiding nonlinear effects in the HPAs and limiting the power per node, the following considerations hold.

1) The proposed LB-MMSE provides a performance identical to MMSE in clear sky. The loss when taking into account additional stochastic losses, which cannot be a priori estimated, is negligible even in harsh conditions, such as the considered NLOS dense-urban case.

2) A federated CF solution shall be selected with VSAT terminals and lower transmission power (i.e., up to 0–2 dBW/MHz). In this case, the achievable spectral efficiency is larger and the increase in the outage is negligible (0.3%–2.1%) in clear-sky conditions, while it is significantly lower in NLOS dense-urban conditions (up to 6.1%). With larger transmission power, a centralized solution shall be preferred.

3) With handheld terminals, centralized beamforming is the best option based on the outage probability (a 0.1–0.2 b/s/Hz increase in the spectral efficiency is not enough to justify a 25% outage) in clear-sky conditions, while in NLOS dense-urban environments, federated solutions with multiple nodes provide an advantage in both the spectral efficiency (0.02–0.2 b/s/Hz) and outage (up to 5.7%), thanks to the spatial diversity at the transmitter.

4) Compared with FR3 and FR4 schemes, the capacity is significantly better with CF-MIMO solutions. When the outage is taken into account, CF-MIMO shall still be selected in the vast majority of the scenarios, with some limited exceptions (e.g., VSAT receivers and low transmission power).

When considering nonideal information at the transmitter, it was observed that the proposed LB-MMSE algorithm:

1) is particularly robust to positioning errors and 2) is significantly impacted by errors on the radiation pattern model. As for the latter, it is worthwhile highlighting that in real deployment scenarios the variance of the amplitude and phase errors on the antenna pattern coefficients is expected to be much lower than 5% as assumed in the above analyses.

Finally, it is worthwhile highlighting, as discussed above, that the benefit introduced by the exploitation of additional nodes in the federated CF-MIMO approach is deeply impacted by the propagation conditions. Based on the extensive numerical results previously discussed, specific scenarios in which the federated architecture is beneficial compared with a standalone node can be identified in terms of the type of terminal (VSAT or handheld), propagation conditions (clear sky, LOS, or NLOS), and propagation environment (suburban, urban, dense urban). Information on the terminal type is available once the UE is connected to the network, while the propagation conditions can be inferred based on: 1) the UE location, i.e., whether the user is in a rural area or in a densely urban environment and 2) a channel quality measure that can be provided by the user based on the received signal power strength on known pilots, e.g., the channel state information reference signal (CSI-RS) in 5G. Thus, the on-ground or on-board network element in charge of scheduling the users and computing the beamforming matrix can identify which users would benefit from the transmission from multiple nodes.

G. Technical Challenges

When considering the implementation of MIMO or CF-MIMO solutions in NTN systems, several challenges arise and shall be properly addressed. Despite not being the main focus of this work, for the sake of completeness, below we discuss the most relevant ones.

1) Notably, the payload design for MIMO architectures shall cope with several constraints in terms of power consumption, hardware cost, and space for electronic

equipment on-board. In this work, we assumed, for each node, a 32×32 UPA, i.e., 1024 radiating elements. Considering that we are operating in *S*-band at 2 GHz with a spacing between adjacent radiating elements equal to 0.55λ, the total array dimension would be $2.64 \times 2.64 = 9 \text{ m}^2$; recently, some industrial endeavors are building and deploying antenna arrays with a dimension of 64 m^2 and, thus, the proposed solution is in line with the near-term developments in payload configurations. The number of radiating elements clearly poses additional challenges, in terms of the beamforming network (BFN) and OBP. In this context, a full digital architecture would require one port per radiating element in the BFN; however, current trends in the electronic equipment are considering the development of BFNs with thousands of ports and, thus, the proposed UPA configuration is feasible in the near future. In terms of power consumption, the most critical aspect is related to the solid state power amplifiers at the transmitter side (the corresponding increase in the power consumption in the BFN and OBP is marginal); in fact, increasing the number of users to be served (or beams, in beam-based systems), the power consumption is increased since the bandwidth per user (beam) is fixed. Thus, depending on the number of signals (beams) to be generated and the overall bandwidth, larger LEO payloads might be required; however, in general a small LEO payload can operate with a few kWs of dc power and, thus, the generation of several tens of beams with 30-MHz bandwidth should not be an issue. An extensive discussion on payload design and architectures can be found in the literature [70].

2) To implement the considered CF-MIMO algorithms, either the CSI or the location shall be estimated by each UE and reported to the network element computing the beamforming matrix. With respect to the former, it is worthwhile highlighting that current NTN systems only support FDD operation, due to the large propagation delays on the NTN channels that make TDD solutions less efficient; as such, it is not possible to exploit channel reciprocity and compute the beamforming matrix based on the uplink channel coefficients. Those shall be in fact adjusted to match the downlink frequency range and this, in turn, introduces a further source of error that can misalign the beamforming and channel matrices, with a detrimental impact on the performance. In this framework, the abovementioned CSI-RS pilots might be used for a pilot aided (PA) estimation. It shall be mentioned that, to allow the estimation of the channel coefficient between each radiating element and the user, these fields shall not be beamformed. It is also worthwhile highlighting that, in the NTN specifications, the estimated CSI are not reported as the real and imaginary parts of the actual channel coefficient, but rather as indicators that allow the transmitter to infer the channel quality or the precoding columns to be used from a precomputed codebook. Thus, when considering CSI-based solutions, the overhead is larger since the PA estimated channel coefficients shall be reported and, possibly, some modifications to the air interface might be needed to allow such reporting. Moreover, in CSI-based algorithms, the estimation of the channel coefficients is usually performed in low-SINR regime, due to the large distance between the satellite(s) and the user, which pose another technical challenge. For location-based solutions, in general the exact location of the UE is not known at RAN level, i.e., at the gNB, but rather at the core network. In addition, the location estimates are usually known with a precision of 2 km. A solution to this challenge could be that of allowing the gNB to have an estimate of the user's location on a geographical grid with a precision not lower than 2 km. As already discussed in this work, the impact of an error on the location estimation in the order of a few km would not significantly impact the performance of LB-MMSE; as for SS-MMSE, the users can limit their feedback to the best serving beam, which also introduces a larger approximation in their location.

3) All algorithms are impacted by the relative movement of the users with respect to the satellite(s). As already discussed, the impact of the users' movement is almost negligible, while that of a moving satellite is more relevant. However, the performance discussed in this work show that a significant benefit can be achieved in the spectral efficiency even when considering moving satellites. In this context, it is worthwhile highlighting that the impact of a moving satellite is larger for larger aging intervals. In general, the scheduling algorithms provide a scheduling matrix defining the users to be served in several consequent time slots. Thus, the larger the number of time slots addressed by the scheduling algorithm, the larger the performance loss compared with an ideal (i.e., fixed) system. These aspects shall be taken into account when designing the scheduling algorithm for the considered constellation.

4) Location-based algorithms require an accurate model of the actual radiation pattern, in order to estimate the radiation in the direction of each user. Previously, we have shown that an error on the radiation pattern model can be detrimental to the performance of such algorithms. The numerical results shown in this work were obtained with a 5% relative amplitude and phase error to assess; such a large error was considered to evaluate the performance in a worst case scenario, while it can be expected that the manufacturing of the radiating elements and the antenna array will lead to much lower impairments. Such manufacturing aspects are not the focus of this work, but shall be properly taken into account by the payload designer.

5) Due to the potentially fast movement of the satellites in NGSO systems, the design and management of handover procedures is one of the most important aspects. In terrestrial systems, the UEs in the service area tend to receive signals with significant power differences from different transmitters; this can be exploited for proper handover procedures based on the received signal strength. In NTN systems, all UEs have a similar distance from the satellite(s) and, thus, only exploiting the received signal strength might not be sufficient. To this aim, mobility enhancements where introduced in 3GPP TS 38.304 [71], for users in connected/idle mode; these include new measurement rules for cell reselection with location and timing information to support conditional handover executed by the UE: 1) location-assisted cell reselection is based on the distance between a UE and the reference location of the cell (serving cell and/or neighbor cell) and 2) timing information refers to the time when the serving cell is going to stop serving a geographical area. The timing and location information associated with a cell are provided via system information. The implementation of handover procedures at swarm level has not yet been addressed in 3GPP NTN. However, it can be expected that similar triggers and procedures can still be implemented; the most relevant modification to be adopted is related to considering time and/or location triggers at swarm level, e.g., the minimum distance between the serving and neighboring swarms or the time at which the last satellite in the serving swarm will be out of visibility. An extensive discussion on network-level and link-level handover procedures, not related to 3GPP NTN specifications, is available in [53].

H. Computational Complexity

In terms of computational complexity, there are two aspects to be considered: 1) the computation of the beamforming matrix and 2) the normalization defining the power distribution. With respect to the former, the following holds.

1) Angeletti and Gaudenzi et al. [64] designed the computationally efficient formulation of MMSE beamforming exploited in (9) and (11). This formulation has a complexity equal to $\mathcal{O}(K^3)$, where K denotes the number of scheduled users in a time slot, and it applies to both CF MMSE and LB-MMSE.
2) For SS-MMSE, the channel matrix has a number of rows equal to the number of beams, N_B, in which the coverage area is spatially sampled. As such, the complexity is given by $\mathcal{O}(N_B^3)$, which is also that of legacy MMSE solutions at beam level.
3) For MB beamforming in (12), to compute the generic (n, ℓ)th coefficient there are two steps: 1) the dot product in the exponential, which has a complexity of $\mathcal{O}(2)$, since both $\mathbf{r}_n$ and $\mathbf{c}_\ell$ are bidimensional position vectors and 2) the computation of the amplitude and

TABLE IV
Computational Complexity of the Beamforming Algorithms

Algorithm	Complexity	Periodicity
MMSE	$\mathcal{O}(K^3)$	time slot
LB-MMSE	$\mathcal{O}(K^3)$	time slot
SS-MMSE	$\mathcal{O}(N_B^3)$	beam layout definition
MB	$\mathcal{O}(N_F)$	beam layout definition

phase of a complex number. As for the amplitude, its complexity is given by the computation of two squares ($\mathcal{O}(2)$), a summation ($\mathcal{O}(2)$) and a square root ($\mathcal{O}(1)$) of bidimensional vectors. Thus, the complexity is $2\mathcal{O}(2) + \mathcal{O}(1) \sim \mathcal{O}(2)$. For the phase, the arc tangent function can be implemented in $\mathcal{O}(1)$. Taking all of these considerations into account, for a single coefficient the complexity is given by $\mathcal{O}(2)$. The number of coefficients to be computed is $N_F N_B$ and, thus, the total complexity of the MB algorithm is $\mathcal{O}(N_F N_B) \sim \mathcal{O}(N_F)$, since typically $N_F \gg N_B$.

Based on the above considerations, as summarized in Table IV, the MB algorithm is the most efficient from a computational complexity perspective. However, it is also the solution providing the worst performance, both in terms of spectral efficiency and outage. The complexity of MMSE or LB-MMSE compared with SS-MMSE is quite similar, assuming that the number of UEs per time slot and the number of beams have similar values.

For the sake of completeness, we also provide the computational complexity of the power distribution approaches previously introduced.

1) For the SPC approach in (14), the complexity is that of the norm of a $K \times K$ matrix, which requires K^2 squares, $K^2 - 1$ summations, and one square root, in addition to a division and another square root. As such, it has a complexity $\mathcal{O}(K^2)$.
2) The MPC solution in (15) requires the following:
   a) the computation of K K-dimensional vector norms, with a complexity of $\mathcal{O}(K)$;
   b) the identification of the maximum element in a K-dimensional array, with a complexity $\mathcal{O}(K)$;
   c) a square root, a multiplication, and a division with complexity $\mathcal{O}(1)$.
   Thus, the overall complexity of MPC is $\mathcal{O}(K)$.
3) For the PAC distribution in (16), we need again to compute the norms of K K-dimensional vectors, with a complexity, $\mathcal{O}(K)$, $K + 1$ divisions, and one square root. As such, the complexity is $\mathcal{O}(K)$.

In terms of power distribution, as summarized in Table V, we can, thus, observe that MPC and PAC are the best options from a computational complexity point of view.

To complete this analysis, it shall also be observed that the MMSE and LB-MMSE beamforming matrices shall be computed at each time slot for the scheduled users; this is motivated by the need to take into account the scheduled

Algorithm	Complexity
SPC	$\mathcal{O}(K^2)$
MPC	$\mathcal{O}(K)$
PAC	$\mathcal{O}(K)$

UEs locations/coefficients. SS-MMSE and MB beamforming are based on a predefined beam lattice, as they refer to the beam centers; as such, the matrices can be precomputed, and then, at a given time slot, the required vectors are combined in a beamforming matrix. Thus, in addition to having a lower computational complexity, these solutions also require the computation only when the beam lattice is defined or redesigned. However, despite this significant advantage, the poor performance in terms of spectral efficiency and outage obtained with MB or SS-MMSE, compared with MMSE and LB-MMSE, does not justify their adoption.

V. STANDARDIZATION ASPECTS

The standardization path of NTN for 5G and beyond systems, and the related timeplan, are extensively discussed in [72], [73], and [74]. For the sake of completeness, in this section, we provide an overview of the 3GPP NTN activities related to the exploitation of distributed antennas and highlight the major challenges that shall be addressed to allow centralized or distributed MIMO via NTN.

The concept of coordination from multiple transmission/reception points (TRPs) has been explored in 3GPP since LTE Rel. 10 (even though the actual features were included from Rel. 11), also building on inter-eNB (through X2 interfaces) signaling to implement intercell interference coordination (ICIC) [75]. In the framework of LTE coordinated multipoint (CoMP), the activities targeted a more dynamic coordination between the TRPs compared with ICIC. It shall be mentioned that, within Rel. 11, there was no specific activity related to the inter-eNB signaling to support CoMP; this led to a generic assumption that ideal backhaul[8] is available, which limited the applicability to either sectors of the same site or network points connected by direct low-latency links. Some extensions were included in Rel. 12 with the introduction of the X2 air interface for exchanging information among eNBs.

Building on these solutions, in 3GPP Rel. 16, further studies were performed to assess the performance and feasibility of noncoherent JT (NC-JT) solutions, i.e., the exploitation of multiple TRPs with more relaxed time and frequency synchronization requirements among the TRPs [76]. In this case, different layers of information are transmitted from multiple nodes; the coordination among the TRPs is either centralized, with a single downlink channel indicator

(DCI) configured for all links, or distributed, with a dedicated DCI per link. Notably, in NC-JT, distributed MIMO is not implemented (being a coherent solution) and, thus, only a power gain from the multiple TRPs is achieved. In general, NC-JT solutions might be beneficial in low-load conditions; this is motivated by observing that, in order to exploit for the same user also the power and resources of a second TRP, it shall be granted that no harmful interference is introduced on other transmissions.

When considering 3GPP NTN systems, multi-TRP solutions (coherent or noncoherent) have not yet been addressed. It might be expected that the first techniques to be designed will belong to the NC-JT category, due to the tight time and frequency synchronization requirements among the cooperating NTN nodes, while coherent JT (C-JT), i.e., federated MIMO, might be addressed in a later phase. It shall be mentioned that, as of today, multi-TRP is not included in Rel. 18 NTN; the topics for Rel. 19 NTN will be finalized in December 2023, but the initial discussions during 3GPP meetings do not seem to prioritize C-JT or NC-JT. Based on these observations, these technologies can be expected to be part of 6G NTN systems, rather than 5G or 5G-A. In fact, future 6G systems will require further increased capacities for which advanced solutions will be needed, such as the centralized or federated MIMO approaches discussed in this work.

VI. CONCLUSION

In this article, we provided a detailed discussion on the design choices allowing the implementation of both federated and centralized CF or beam-based MIMO solutions in NTN NGSO constellations; both regenerative, with functional split options, and transparent payloads were addressed, as well as OGBF and OBBF solutions. A detailed description of the architecture options, with the related challenges and benefits, has been reported. Then, we designed: 1) a novel location-based CF-MIMO algorithm for NTN NGSO constellations, which is completely user-centric, i.e., tailored to the actual users' locations and 2) novel power normalization approaches for federated MIMO algorithms that can be applied to swarms of NGSO nodes. The outcomes of the extensive numerical results showed that: 1) the proposed LB-MMSE algorithm provides a performance close to the CSI-based MMSE, but with a significantly reduced overhead and complexity at the terminal side and 2) federated CF-MIMO solutions over NGSO swarms provide benefits with VSAT terminals and low transmission power, and with handheld terminals in NLOS dense-urban conditions. The performance was assessed also considering three and four colors frequency reuse schemes; it was shown that, apart from VSAT terminals and low transmission power, the CF-MIMO paradigm provides a significant performance improvement. The robustness of the considered location-based algorithms was assessed with nonideal location estimation and nonideal knowledge of the actual radiation of the on-board UPA elements, with respect to their mathematical model. It was shown that the former

---

[8]It shall be noticed that, in 3GPP, ideal backhaul refers to having ideal time and frequency synchronization among the multiple TRPs and not to actual backhaul links.

does not pose issues, while the latter is more critical. Finally, the various algorithms and power distribution solutions have been compared also in terms of their computational complexity; it was observed that SS-MMSE and MB beamforming require a lower complexity, in addition to the possibility of being precomputed. However, the poor performance in spectral efficiency and outage observed in the numerical assessment does not justify their adoption over MMSE or LB-MMSE. In terms of power distribution, the MPC solution is the one with the lower complexity, in addition to being the approach that guarantees all on-board amplifiers to operate in the linear regime. Future developments of this work include the analysis of the tight synchronization among the swarm nodes for federated CF-MIMO and the performance assessment with variable UPA configurations and more than two nodes per swarm; moreover, also heterogeneous scenarios with nodes flying at different orbits, or with different payload configurations, might be considered.

ACKNOWLEDGMENT

REFERENCES

[1] W. Jiang, B. Han, M. A. Habibi, and H. D. Schotten, "The road towards 6G: A comprehensive survey," *IEEE Open J. Commun. Soc.*, vol. 2, pp. 334–366, 2021.

[2] O. Kodheli et al., "Satellite communications in the new space era: A survey and future challenges," *IEEE Commun. Surv. Tut.*, vol. 23, no. 1, pp. 70–109, Jan./Mar. 2021.

[3] M. Giordani, M. Polese, M. Mezzavilla, S. Rangan, and M. Zorzi, "Toward 6G networks: Use cases and technologies," *IEEE Commun. Mag.*, vol. 58, no. 3, pp. 55–61, Mar. 2020.

[4] J. R. Bhat and S. A. Alqahtani, "6G ecosystem: Current status and future perspective," *IEEE Access*, vol. 9, pp. 43134–43167, 2021.

[5] ITU-R WP 5D, "Workshop on "IMT for 2030 and beyond"," Jun. 2022, https://www.itu.int/en/ITU-R/study-groups/rsg5/rwp5d/Pages/wsp-imt-vision-2030-and-beyond.aspx

[6] "Representative use cases and key network requirements for network, 2030," Tech. Rep. ITU-T FG-NET-2030, Jan. 2020. [Online]. Available: https://www.itu.int/dms_pub/itu-t/opb/fg/T-FG-NET2030-2020-SUB.G1-PDF-E.pdf

[7] "Network 2030 - A blueprint of technology, applications and market drivers towards the year 2030 and Beyond," ITU-R, White Paper ITU-R FG-NET-2030, 2019. [Online]. Available: https://www.itu.int/en/ITU-T/focusgroups/net2030/Documents/White_Paper.pdf

[8] "Network 2030 architecture framework," Technical Specification ITU-R FG-NET-2030, 2020. [Online]. Available: https://www.itu.int/en/ITU-T/focusgroups/net2030/Documents/Network_2030_Architecture-framework.pdf

[9] 5G-IA White Paper, "European vision for the 6G network ecosystem," Jun. 2021, doi: 10.5281/zenodo.5007671.

[10] M. Hosseinian, J. P. Choi, S.-H. Chang, and J. Lee, "Review of 5G NTN standards development and technical challenges for satellite integration with the 5G network," *IEEE Aerosp. Electron. Syst. Mag.*, vol. 36, no. 8, pp. 22–31, Aug. 2021.

[11] H. Kokkinen, A. Piemontese, L. Kulacz, F. Arnal, and C. Amatetti, "Coverage and interference in co-channel spectrum sharing between terrestrial and satellite networks," in *Proc. IEEE Aerosp. Conf.*, 2023, pp. 1–9.

[12] S. Liu et al., "LEO satellite constellations for 5G and beyond: How will they reshape vertical domains?," *IEEE Commun. Mag.*, vol. 59, no. 7, pp. 30–36, Jul. 2021.

[13] L. Boero, R. Bruschi, F. Davoli, M. Marchese, and F. Patrone, "Satellite networking integration in the 5G ecosystem: Research trends and open challenges," *IEEE Netw.*, vol. 32, no. 5, pp. 9–15, Sep./Oct. 2018.

[14] A. Guidotti et al., "Architectures and key technical challenges for 5G systems incorporating satellites," *IEEE Trans. Veh. Technol.*, vol. 68, no. 3, pp. 2624–2639, Mar. 2019.

[15] A. Guidotti et al., "Architectures, standardisation, and procedures for 5G satellite communications: A survey," *Comput. Netw.*, vol. 183, 2020, Art. no. 107588.

[16] A. Kyrgiazos, B. Evans, P. Thompson, T. Mathiopoulos, and S. Papaharalabos, "A terabit/second satellite system for European broadband access: A feasibility study," *Int. J. Satell. Commun. Netw.*, vol. 32, no. 2, pp. 63–92, 2014, doi: 10.1002/sat.1067.

[17] E. Feltrin, J. Freixe, and E. Weller, "Mobility in Ku and Ka bands: The Eutelsat's point of view," in *Proc. 5th Eur. Conf. Antennas Propag.*, 2011, pp. 2336–2340.

[18] A. I. Pérez-Neira, M. Á. Vázquez, S. Maleki, M. R. B. Shankar, and S. Chatzinotas, "Signal processing for high throughput satellite systems: Challenges in new interference-limited scenarios," 2018. [Online]. Available: http://arxiv.org/abs/1802.03958

[19] P. Wang, B. Di, and L. Song, "Mega-constellation design for integrated satellite-terrestrial networks for global seamless connectivity," *IEEE Wireless Commun. Lett.*, vol. 11, no. 8, pp. 1669–1673, Aug. 2022.

[20] G. M. Capez et al., "Characterization of mega-constellation links for LEO missions with applications to EO and ISS use cases," *IEEE Access*, vol. 11, pp. 25616–25628, 2023.

[21] N. Wang, L. Liu, Z. Qin, B. Liang, and D. Chen, "Capacity analysis of LEO mega-constellation networks," *IEEE Access*, vol. 10, pp. 18420–18433, 2022.

[22] V. Icolari, A. Guidotti, D. Tarchi, and A. Vanelli-Coralli, "An interference estimation technique for satellite cognitive radio systems," in *Proc. IEEE Int. Conf. Commun.*, 2015, pp. 892–897.

[23] S. Chatzinotas et al., "Cognitive approaches to enhance spectrum availability for satellite systems," *Int. J. Satell. Commun. Netw.*, vol. 35, no. 5, pp. 407–442, 2017, doi: 10.1002/sat.1197.

[24] G. Caire et al., "Perspectives of adopting interference mitigation techniques in the context of broadband multimedia satellite systems," in *Proc. 23rd AIAA Int. Commun. Satell. Syst. Conf.*, 2005, pp. 1–8.

[25] P.-D. Arapoglou, K. Liolis, M. Bertinelli, A. Panagopoulos, P. Cottis, and R. De Gaudenzi, "MIMO over satellite: A review," *IEEE Commun. Surv. Tut.*, vol. 13, no. 1, pp. 27–51, Jan./Mar. 2011.

[26] N. Zorba, M. Realp, and A. I. Perez-Neira, "An improved partial CSIT random beamforming for multibeam satellite systems," in *Proc. 10th Int. Workshop Signal Process. Space Commun.*, 2008, pp. 1–8.

[27] P.-D. Arapoglou et al., "DVB-S2X-enabled precoding for high throughput satellite systems," *Wiley Int. J. Satell. Commun. Netw.*, vol. 34, no. 3, pp. 439–455, Jun. 2015.

[28] D. Christopoulos, P.-D. Arapoglou, and S. Chatzinotas, "Linear precoding in multi-beam SatComs: Practical constraints," in *Proc. 31st AIAA Int Commun Satell. Syst. Conf.*, 2013, pp. 1–9.

[29] G. Zheng, S. Chatzinotas, and B. Ottersten, "Generic optimization of linear precoding in multibeam satellite systems," *IEEE Trans. Wireless Commun.*, vol. 11, no. 6, pp. 2308–2320, Jun. 2012.

[30] D. Christopoulos et al., "Multibeam joint precoding: Frame-based design," in *Cooperative and Cognitive Satellite Systems*, S. Chatzinotas, B. Ottersten, and R. De Gaudenzi, Eds. New York, NY, USA: Academic, 2015, ch. 3, pp. 83–118.

[31] M. Poggioni, M. Berioli, and P. Banelli, "Ber performance of multibeam satellite systems with Tomlinson-Harashima precoding," in *Proc. IEEE Int. Conf. Commun.*, 2009, pp. 1–6.

[32] S. Chatzinotas, G. Zheng, and B. Ottersten, "Joint precoding with flexible power constraints in multibeam satellite systems," in *Proc. IEEE Glob. Telecommun. Conf.*, 2011, pp. 1–5.

[33] V. Joroughi, M. B. Shankar, S. Maleki, S. Chatzinotas, J. Grotz, and B. Ottersten, "On-board precoding in a multiple gateway multibeam satellite system," in *Proc. IEEE 88th Veh. Technol. Conf.*, 2018, pp. 1–5.

[34] A. Guidotti and A. Vanelli-Coralli, "Design trade-off analysis of precoding multi-beam satellite communication systems," in *Proc. IEEE Aerosp. Conf.*, 2021, pp. 1–12.

[35] P. J. Honnaiah, E. Lagunas, N. Maturo, and S. Chatzinotas, "Demand-aware beam design and user scheduling for precoded multibeam Geo satellite systems," in *Proc. 25th Int. ITG Workshop Smart Antennas*, 2021, pp. 1–6.

[36] F. Ortiz, E. Lagunas, and S. Chatzinotas, "Unsupervised learning for user scheduling in multibeam precoded GEO satellite systems," in *Proc. Joint Eur. Conf. Netw. Commun. 6G Summit*, 2022, pp. 190–195.

[37] A. Guidotti, C. Amatetti, F. Arnal, B. Chamaillard, and A. Vanelli-Coralli, "Location-assisted precoding in 5G LEO systems: Architectures and performances," in *Proc. Joint Eur. Conf. Netw. Commun. 6G Summit*, 2022, pp. 154–159, doi: 10.1109/EuCNC/6GSummit54941.2022.9815611.

[38] G. Taricco, "Linear precoding methods for multi-beam broadband satellite systems," in *Proc. 20th Eur. Wireless Conf.*, 2014, pp. 1–6.

[39] B. Devillers, A. Perez-Neira, and C. Mosquera, "Joint linear precoding and beamforming for the forward link of multi-beam broadband satellite systems," in *Proc. IEEE Glob. Telecommun. Conf.*, 2011, pp. 1–6.

[40] Y. C. B. Silva and A. Klein, "Linear transmit beamforming techniques for the multigroup multicast scenario," *IEEE Trans. Veh. Technol.*, vol. 58, no. 8, pp. 4353–4367, Oct. 2009.

[41] M. A. Vazquez et al., "Precoding in multibeam satellite communications: Present and future challenges," *IEEE Wireless Commun.*, vol. 23, no. 6, pp. 88–95, Dec. 2016.

[42] D. Christopoulos, S. Chatzinotas, and B. Ottersten, "Weighted fair multicast multigroup beamforming under per-antenna power constraints," *IEEE Trans. Signal Process.*, vol. 62, no. 19, pp. 5132–5142, Oct. 2014.

[43] V. Joroughi, M. A. Vazquez, and A. I. Perez-Neira, "Generalized multicast multibeam precoding for satellite communications," *IEEE Trans. Wireless Commun.*, vol. 16, no. 2, pp. 952–966, Feb. 2017, doi: 10.1109/TWC.2016.2635139.

[44] M. A. Vazquez et al., "Precoding, scheduling, and link adaptation in mobile interactive multibeam satellite systems," *IEEE J. Sel. Areas Commun.*, vol. 36, no. 5, pp. 971–980, May 2018.

[45] A. Liu et al., "Robust multigroup multicast precoding for frame-based multi-beam satellite communications," in *Proc. IEEE 29th Annu. Int. Symp. Pers., Indoor, Mobile Radio Commun.*, 2018, pp. 1237–1241.

[46] A. Guidotti and A. Vanelli-Coralli, "Clustering strategies for multicast precoding in multibeam satellite systems," *Wiley Int. J. Satell. Commun. Netw.*, vol. 38, no. 2, pp. 85–104, Jul. 2019.

[47] A. Guidotti and A. Vanelli-Coralli, "Geographical scheduling for multicast precoding in multi-beam satellite systems," in *Proc. 9th Adv. Satell. Multimedia Syst. Conf., 15th Signal Process. Space Commun. Workshop*, 2018, pp. 1–8.

[48] A. Guidotti, C. Sacchi, and A. Vanelli-Coralli, "Feeder link precoding for future broadcasting services: Architecture and performance," *IEEE Trans. Aerosp. Electron. Syst.*, vol. 58, no. 4, pp. 3126–3146, Aug. 2022.

[49] T. Delamotte, R. T. Schwarz, K.-U. Storek, and A. Knopp, "MIMO feeder links for high throughput satellites," in *Proc. 22nd Int. ITG Workshop Smart Antennas*, 2018, pp. 1–8.

[50] T. Delamotte, K.-U. Storek, and A. Knopp, "MIMO processing for satellites in the 5G era," in *Proc. IEEE 2nd 5G World Forum*, 2019, pp. 629–635.

[51] D. Tuzi, T. Delamotte, and A. Knopp, "Beamforming performance of satellite swarm-based antenna arrays for 6G direct-to-cell connectivity," in *Proc. 26th Int. ITG Workshop Smart Antennas, 13th Conf. Syst., Commun., Coding*, 2023, pp. 1–6.

[52] D. Tuzi, T. Delamotte, and A. Knopp, "Satellite swarm-based antenna arrays for 6G direct-to-cell connectivity," *IEEE Access*, vol. 11, pp. 36907–36928, 2023.

[53] M. Y. Abdelsadek, G. K. Kurt, and H. Yanikomeroglu, "Distributed massive MIMO for LEO satellite networks," *IEEE Open J. Commun. Soc.*, vol. 3, pp. 2162–2177, 2022.

[54] Y. Omid, Z. M. Bakhsh, F. Kayhan, Y. Ma, and R. Tafazolli, "Space MIMO: Direct unmodified handheld to multi-satellite communication," 2023, *arXiv:2305.19049*.

[55] F. Riera-Palou, G. Femenias, M. Caus, M. Shaat, and A. I. Pérez-Neira, "Scalable cell-free massive MIMO networks with leo satellite support," *IEEE Access*, vol. 10, pp. 37557–37571, 2022.

[56] E. G. Larsson, O. Edfors, F. Tufvesson, and T. L. Marzetta, "Massive MIMO for next generation wireless systems," *IEEE Commun. Mag.*, vol. 52, no. 2, pp. 186–195, Feb. 2014.

[57] H. Q. Ngo, A. Ashikhmin, H. Yang, E. G. Larsson, and T. L. Marzetta, "Cell-free massive MIMO versus small cells," *IEEE Trans. Wireless Commun.*, vol. 16, no. 3, pp. 1834–1850, Mar. 2017.

[58] Q. N. Le, V.-D. Nguyen, O. A. Dobre, N.-P. Nguyen, R. Zhao, and S. Chatzinotas, "Learning-assisted user clustering in cell-free massive MIMO-NOMA networks," *IEEE Trans. Veh. Technol.*, vol. 70, no. 12, pp. 12872–12887, Dec. 2021.

[59] N. Rajapaksha, K. B. S. Manosha, N. Rajatheva, and M. Latva-aho, "Deep learning-based power control for cell-free massive MIMO networks," in *Proc. IEEE Int. Conf. Commun.*, 2021, pp. 1–7.

[60] 3GPP, "Study on new radio access technology: Radio access architecture and interfaces," Tech. Rep. 38.801, Apr. 2017.

[61] 3GPP, "NG-RAN; F1 general aspects and principles," TS 38.470, Jun. 2023.

[62] 3GPP, "Study on New Radio (NR) to support non-terrestrial networks (Release 15)," Tech. Rep. 38.811, Sep. 2020.

[63] 3GPP, "Study on new radio access technology: Radio Frequency (RF) and co-existence aspects (Release 14)," Tech. Rep. 38.803, Sep. 2017.

[64] P. Angeletti and R. De Gaudenzi, "A pragmatic approach to massive MIMO for broadband communication satellites," *IEEE Access*, vol. 8, pp. 132212–132236, 2020.

[65] R. Muharar and J. Evans, "Downlink beamforming with transmit-side channel correlation: A large system analysis," in *Proc. IEEE Int. Conf. Commun.*, 2011, pp. 1–5.

[66] 3GPP, "Solutions for NR to support non-terrestrial networks (NTN) (Release 16)," Tech. Rep. 38.821, May 2021.

[67] "Modelling and simulation of IMT networks and systems for use in sharing and compatibility studies," ITU-R Recommendation M.2101, Feb. 2017.

[68] 3GPP, "NR; Satellite Access Node radio transmission and reception (Release 17)," Tech. Rep. 38.108, Jun. 2022.

[69] 3GPP, "Study on using satellite access in 5G," Tech. Rep. 22.822, Jul. 2018.

[70] A. Mengali, A. Ginesi, and S. D'Addio, "Computer-aided payload architecture optimization for HTS satellites," in *Proc. 10th Adv. Satell. Multimedia Syst. Conf., 16th Signal Process. Space Commun. Workshop*, 2020, pp. 1–8, doi: 10.1109/ASMS/SPSC48805.2020.9268888.

[71] 3GPP, "NR; User Equipment (UE) procedures in idle mode and in RRC Inactive state," TS 38.304, Jul. 2023.

[72] A. Guidotti et al., "The path to 5G-advanced and 6G non-terrestrial network systems," in *Proc. 11th Adv. Satell. Multimedia Syst. Conf., 17th Signal Process. Space Commun. Workshop*, 2022, pp. 1–8.

[73] M. El Jaafari and N. Chuberre, "Guest editorial IJSCN special issue on 3GPP NTN standards for future satellite communications," *Int. J. Satell. Commun. Netw.*, vol. 41, no. 3, pp. 217–219, 2023. [Online]. Available: https://onlinelibrary.wiley.com/doi/abs/10.1002/sat.1472

[74] M. El Jaafari, N. Chuberre, S. Anjuere, and L. Combelles, "Introduction to the 3GPP-defined NTN standard: A comprehensive view on the 3GPP work on NTN," *Int. J. Satell. Commun. Netw.*, vol. 41, no. 3, pp. 220–238, 2023. [Online]. Available: https://onlinelibrary.wiley.com/doi/abs/10.1002/sat.1471

[75] E. Dahlman, S. Parkvall, and J. Sköld, "Multi-point coordination and transmission," in *4G LTE-Advanced Pro and The Road to 5G*, 3rd ed., E. Dahlman, S. Parkvall, and J. Sköld, Eds. New York, NY, USA: Academic Press, 2016, ch. 13, pp. 331–345. [Online]. Available: https://www.sciencedirect.com/science/article/pii/B9780128045756000133

[76] M. Khoshnevisan, K. Jayasinghe, R. Chen, A. Davydov, and L. Guo, "Enhanced reliability and capacity with multi-TRP transmission," *IEEE Commun. Standards Mag.*, vol. 6, no. 1, pp. 13–19, Mar. 2022.

Alessandro Vanelli-Coralli (Senior Member, IEEE) received the Dr.Ing. degree in electronics engineering and the Ph.D. degree in electronics and computer science from the University of Bologna, Bologna, Italy, in 1991 and 1996, respectively.

In 1996, he joined the University of Bologna, where he is currently a Full Professor. From 2003 to 2005, he was a Visiting Scientist with Qualcomm Inc., San Diego, CA, USA. From 2013 to 2018, he chaired the Ph.D. Board, Electronics, Telecommunications, and Information Technologies. He participated in national and international research projects on wireless and satellite communication systems and he has been a Project Coordinator and Scientific Responsible for several European Space Agency and European Commission funded projects. He is currently the Responsible for the Vision and Research Strategy task force of the NetworldEurope SatCom Working Group.

Dr. Vanelli-Coralli is a Member of the Editorial Board of the Wiley InterScience Journal on *Satellite Communications and Networks* and an Associate Editor of the Editorial Board of *Aerial and Space Networks* Frontiers in Space Technologies. He was with the organization committees of scientific conferences, and since 2010, he has been the general Co-Chairman of the IEEE Advanced Satellite Multimedia Systems Conference. He was the recipient of several Best Paper Awards and 2019 IEEE Satellite Communications Technical Recognition Award.

Alessandro Guidotti (Member, IEEE) received the master's degree (magna cum laude) in telecommunications engineering and the Ph.D. degree in electronics, computer science, and telecommunications from the University of Bologna, Bologna, Italy, in 2008 and 2012, respectively.

From 2009 to 2011, he was a Representative for the Italian Administration within CEPT SE43. During 2011 and 2012, he was a Visiting Researcher with SUPELEC, Paris, France. From 2014 to 2021, he was a Research Associate with the Department of Electrical, Electronic, and Information Engineering "Guglielmo Marconi," University of Bologna. From 2021, he has been a Researcher with the Consorzio Interuniversitario delle Telecomunicazioni, located at the Research Unit of the University of Bologna. He is active in national and international research projects on wireless and satellite communication systems in several European Space Agency and European Commission funded projects. His research interests include wireless communication systems, spectrum management, cognitive radios, interference management, 5G, and machine learning.

Dr. Guidotti is currently a Member of the Editorial Board as a Review Editor of the *Aerial and Space Networks* journal for Frontiers in Space Technologies. Since 2018, he has been a TPC and Publication Co-Chair with the ASMS/SPSC Conference. He is a Workshop Co-Chair of the 2023 IEEE International Conference on Wireless for Space and Extreme Environments and a Member of IEEE Aerospace and Electronic Systems Society "Glue Technologies for Space Systems" Technical Panel.

Carla Amatetti (Member, IEEE) received the M.Sc. degree in communications and computer network engineering from the Politecnico of Torino, Turin, Italy, in 2018, and the Ph.D. degree in electronics, telecommunications, and information technologies engineering from the University of Bologna, Bologna, Italy, in 2023.

From 2018 to 2019, she was with the Fiat Research Center, Turin, on activities related to 5G for vehicular applications. In November 2019, she joined the Digicomm group within the Department of Electrical, Electronic, and Information Engineering, University of Bologna, as a Ph.D. student. During the Ph.D. period, she spent seven months with the University of Luxembourg, Esch-sur-Alzette, Luxembourg, to carry out research on NB-IoT via NTN. Since October 2023, she has been a Junior Assistant Professor with the University of Bologna. She was with different international and national funded initiatives on the integration between terrestrial and nonterrestrial networks. Her research interests include nonterrestrial networks, NB-IoT, 5G, and 6G networks at physical and medium access control layers.